THE ANTENNA LABORATORY

RESEARCH ACTIVITIES in ---

Automata Controls *Antennas* *Echo Area Studies*
Microwave Circuits *Astronautics* *E M Field Theory*
Terrain Investigations *Radomes* *Systems Analysis*
Wave Propagation *Submillimeter Applications*

A Physical Optics Approximation of the Scattering for Axial Incidence from Rotationally Symmetric Targets

by

David L. Moffatt

Contract AF 30(602)-2042

925-6 15 February 1961

Department of ELECTRICAL ENGINEERING

THE OHIO STATE UNIVERSITY
RESEARCH FOUNDATION
Columbus, Ohio

REPORT 925-6

REPORT
by
THE OHIO STATE UNIVERSITY RESEARCH FOUNDATION
COLUMBUS 12, OHIO

Cooperator	Rome Air Development Center Air Research and Development Command Griffiss Air Force Base, New York
Contract	AF 30(602)-2042
Investigation of	Countermeasures Against Radar Absorbing Materials
Subject of Report	A Physical Optics Approximation of the Scattering for Axial Incidence from Rotationally Symmetric Targets
Submitted by	David L. Moffatt Antenna Laboratory Department of Electrical Engineering
Date	15 February 1961

TABLE OF CONTENTS

ABSTRACT

A physical optics approximation to the monostatic and bistatic scattering for axial incidence from rotationally symmetric targets is developed. Both conducting and lossy dielectric bodies, characterized by a surface impedance equal to the intrinsic impedance of the scattering medium, are treated. The resulting general expressions, which are valid within the physical optics approximation for any rotationally symmetric target, are specialized to long, thin, shapes, either finite with sharp apices or semi infinite with a sharp apex, by a modification of the normal physical optics approximation.

Theoretical calculations of the axial back scatter from spheres, double cones, parabolic ogives, semi-infinite cones, and semi-infinite cylinders with conical caps for several values of the scatterer surface impedance are presented. Theoretical calculations of the bistatic E plane (plane of the incident E field) cross-section of conducting semi-infinite cones, double cones, and semi-infinite cylinders with conical caps are also given. Where possible, the theoretical results are compared with the exact solution or with representative experimental data to indicate the validity of the theory.

CHAPTER I
INTRODUCTION

The scattering of a plane, monochromatic, electromagnetic wave incident on perfectly conducting targets as predicted by the physical optics approximation has been developed previously for both the monostatic,[1] and bistatic[2] situations. Little has been done however, in the development of simple approximate solutions to the scattering from imperfectly conducting targets. Further, the standard physical optics results fail, in general, to take into account the shadow region of the scatterer. Application of these results then to long, thin shapes show considerable deviation from experimental data,[4] even for targets of a size generally considered to be within the physical optics range. The scattering from long, thin shapes has been of interest recently,[3,4] both as an approximation to the scattering cross section of missile type targets, and as a study of inherently low-reflection shapes possibly applicable to the camouflage of targets by shaping for minimum radar return.

The present investigation was inspired by the work of Adachi,[3] who derived the back-scattering cross-section along the symmetry axis of finite and semi-infinite bodies of revolution using a variational technique. The success of this derivation in predicting the axial backscatter from symmetric and non-symmetric double

cones encouraged the present extension to bistatic scattering cross-sections and to imperfectly conducting targets. Since, when certain simplifying assumptions are made, Adachi's solution reduces as a first order approximation to the physical optics result where the physical optics currents are assumed over the entire scatterer surface rather than just the illuminated portion, it was felt that an extension of the results to imperfectly conducting scatterers and bistatic cross-sections could be made using this modified physical optics approximation and the radiation integral.[6]

In this report, general expressions are derived for the monostatic and bistatic scattering cross-sections for axial incidence on rotationally symmetric targets with an arbitrary surface impedance. The physical optics approximation and the radiation integral are used. These results are then modified for long, thin targets which are either finite with two sharp apices or semi-infinite with one sharp apex. It is shown that this modification removes the polarization dependence of the expressions for the bistatic cross-sections for the perfectly conducting target. Experimental evidence indicates that the modified results are valid in the E-plane for long, thin targets.

A variational solution for the forward scatter from conducting targets of the long, thin class is derived to supplement the physical optics results.

The following theoretical calculations are presented:

a. Axial backscatter from spheres, double cones, semi-infinite cones, and semi-infinite cylinders with conical and ogival caps for ratios of the surface impedance of the scatterer to the free-space impedance of 0, 0.25, 0.5, and 0.75;

b. Bistatic E-plane scattering cross-sections of conducting semi-infinite cones, double cones, and semi-infinite cylinders with conical caps.

The exact solution for the backscatter from spheres under impedance boundary conditions, and experimental measurements of the monostatic and bistatic cross sections of symmetric double cones are also given to indicate the limits of validity of the theory.

The report concludes with a discussion of applications of the derived equations, some general conclusions concerning the scattering from rotationally symmetric targets, and a summary of the significant results.

In the Appendix, certain integrals encountered in the calculation of bistatic cross-sections of double cones are evaluated, and curves of a tabulated integral, which were used for interpolation, are presented.

CHAPTER II
DERIVATION OF THE SCATTERING CROSS-SECTIONS

The cylindrical coordinate system R,ϕ, z to be used in this development is shown in Fig. 1. The rotational axis of symmetry of

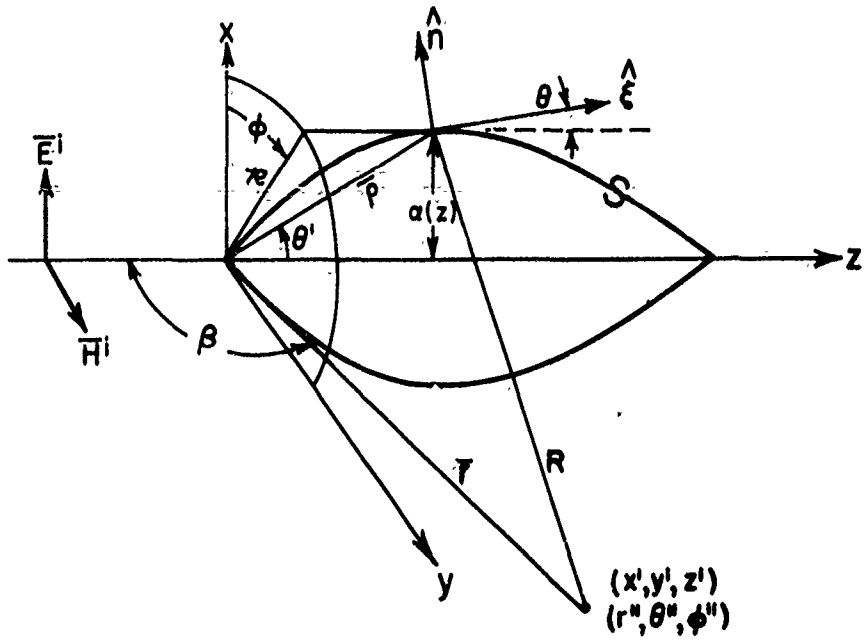

Fig. 1. Cylindrical coordinate system.

the target is coincident with the z axis, and the target shape is described by the radius, $\alpha(z)$, as a function of z. The unit vector $\hat{\xi}$ is a tangential generating element of the scatterer and $\hat{z} \cdot \hat{\xi} = \cos\theta$. The unit normal to the target surface is $\hat{n}$ and $\vec{\rho}$ is the position vector (from origin) of a surface element ds. The target has the constitutive constants μ and ϵ, the complex permeability and permittivity, respectively.

From Stratton,[6] using an $e^{-j\omega t}$ time convention, the magnetic field scattered at a point x', y', z' exterior to the closed surface, S, due to an incident field $\bar{E}^i$, $\bar{H}^i$ on S in terms of surface currents only is given by

$$(1) \qquad \bar{H}^s = \frac{j}{4\pi\omega\mu} \iint_s \nabla \times \nabla \times \left[\frac{e^{jkR}}{R} \bar{E}^T \times \hat{n} \right] ds + \frac{1}{4\pi} \iint_s \nabla \times \left(\frac{e^{jkR}}{R} \hat{n} \times \bar{H}^T \right) ds,$$

where $\hat{n}$ is a unit outward normal to S, $\bar{E}^T$ and $\bar{H}^T$ are the total electric and magnetic fields on S and ∇ operates only on the field points. Using the vector identities,[7]

$$(2) \qquad \nabla \times \phi\bar{a} = \nabla\phi \times \bar{a} + \hat{\phi} \nabla \times \bar{a},$$

$$\nabla \times (\bar{a} \times \bar{b}) = \bar{a} \nabla \cdot \bar{b} - \bar{b} \nabla \cdot \bar{a} + (\bar{b} \cdot \nabla)\bar{a} - (\bar{a} \cdot \nabla)\bar{b},$$

then

$$(3) \qquad \nabla \times \left[\frac{e^{jkR}}{R} (\hat{n} \times \bar{H}^T) \right] = \nabla \frac{e^{jkR}}{R} \times (\hat{n} \times \bar{H}^T),$$

$$(4) \qquad \nabla \times \left[\frac{e^{jkR}}{r} (\bar{E}^T \times \hat{n}) \right] = \nabla \frac{e^{jkR}}{R} \times (\bar{E}^T \times \hat{n}),$$

and

$$(5) \qquad \nabla \times \nabla \frac{e^{jkR}}{R} \times (\bar{E}^T \times \hat{n}) = -(\bar{E}^T \times \hat{n}) \nabla^2 \frac{e^{jkR}}{R} + \left\{ (\bar{E}^T \times \hat{n} \cdot \hat{R}) \frac{\partial}{\partial R} \right\} \cdot \nabla \frac{e^{jkR}}{R}.$$

In the far field,

$$\nabla^2 \frac{e^{jkR}}{R} \simeq -k^2 \frac{e^{jkr}}{r} e^{-jk(\bar{p} \cdot \hat{r})},$$

$$\nabla \frac{e^{jkR}}{R} \simeq \hat{r} jk \frac{e^{jkr}}{r} e^{-jk(\bar{p} \cdot \hat{r})} , \tag{6}$$

where $\hat{r}$ is a unit vector in the direction of the point x', y', z'.

From (3), (4), (5) and (6) then,

$$\bar{H}^s = \frac{jk^2 e^{jkr}}{4\pi \omega \mu r} \iint_s \left[(\bar{E}^T \times \hat{n}) - \hat{r}(\bar{E}^T \times \hat{n} \cdot \hat{r}) \right] e^{-jk(\bar{p} \cdot \hat{r})} ds \tag{7}$$

$$\frac{+jke^{jkr}}{4\pi r} \iint_s \hat{r} \times (\hat{n} \times \bar{H}^T) e^{-jk(\bar{p} \cdot \hat{r})} ds.$$

Let the plane, monochromatic, incident wave propagating in the z direction be given by,

$$\bar{E}^i = \hat{x} e^{j(kz-\omega t)},$$

$$\bar{H}^i = \frac{\hat{y}}{z_o} e^{j(kz-\omega t)}. \tag{8}$$

z_o is the intrinsic impedance of free space, and k is the free space wavenumber. The plane of incidence is defined by $\hat{n}$ and the z axis. At each point on the surface of the target the incident field is separated into components in and normal to the plane of incidence. If subscripts 1 and 2 denote components in and normal to the incident plane respectively, then with the factor $e^{-j\omega t}$ understood,

$$\bar{E}_1^i = \hat{\alpha} \cos\phi \, e^{-jkz}$$

(9)

$$\bar{H}_1^i = \hat{\beta} \frac{\cos\phi}{z_o} e^{jkz} \quad ,$$

$$\bar{E}_2^i = -\hat{\beta} \sin\phi \, e^{jkz}$$

(10)

$$\bar{H}_2^i = \frac{\hat{\alpha} \sin\phi}{z_o} e^{jkz} \quad ,$$

where

$$\hat{\alpha} = \hat{x} \cos\phi + \hat{y} \sin\phi$$

(11)

$$\hat{\beta} = -\hat{x} \sin\phi + \hat{y} \cos\phi \ .$$

On the surface S, the scattered fields are given approximately by

$$\bar{E}^s = R_{\parallel} \bar{E}_1^i + R_{\perp} \bar{E}_2^i \ ,$$

(12)

$$\bar{H}^s = -R_{\parallel} \bar{H}_1^i - R_{\perp} \bar{H}_2^i \ ,$$

where $R_{\parallel}$ and $R_{\perp}$ are the plane sheet reflection coefficients for polarizations in and normal to the plane of incidence, respectively. Equation (12) is the physical optics approximation on the illuminated portion of the scatterer or the modified physical optics approximation over the entire scatterer, as will be seen later. Thus, on the surface, S, the total fields are given by,

$$
\begin{aligned}
\bar{E}_1^T &= \bar{E}_1^i + \bar{E}_1^s = \hat{\alpha}\,[1+R_{\parallel}]\cos\phi\; e^{jkz} \\
\bar{E}_2^T &= \bar{E}_2^i + \bar{E}_2^s = -\hat{\beta}\,[1+R_{\perp}]\sin\phi\; e^{jkz} \\
\bar{H}_1^T &= \bar{H}_1^i + \bar{H}_1^s = \hat{\beta}\,[1-R_{\parallel}]\,\frac{\cos\phi}{z_o}\; e^{jkz} \\
\bar{H}_2^T &= \bar{H}_2^i + \bar{H}_2^s = \hat{\alpha}\,[1-R_{\perp}]\,\frac{\sin\phi}{z_o}\; e^{jkz}
\end{aligned}
\tag{13}
$$

Using the coordinate description shown in Fig. 1,

$$
\hat{n}\times\bar{E}_1^T = [\hat{x}\sin\phi - \hat{y}\cos\phi]\sin\theta\cos\phi\,[1+R_{\parallel}]e^{jkz}\;, \tag{14}
$$

$$
\hat{n}\times\bar{E}_2^T = -[\hat{x}\sin\theta\cos\phi + \hat{y}\sin\theta\sin\phi + \hat{z}\cos\theta]\sin\phi[1+R_{\perp}]\cdot e^{jkz}\;, \tag{15}
$$

$$
\hat{n}\times(\hat{n}\times\bar{H}_1^T) = \{\hat{x}\sin\phi - \hat{y}\cos\phi\}\,[1-R_{\parallel}]\,\frac{\cos\phi}{z_o}\; e^{jkz}\;, \tag{16}
$$

$$
\hat{n}\times(\hat{n}\times\bar{H}_2^T) = -\{\hat{x}\sin\theta\cos\phi + \hat{y}\sin\theta\sin\phi + \hat{z}\cos\theta\}\,\frac{\sin\theta\sin\phi}{z_o}\,[1-R_{\perp}]e^{jkz}\;, \tag{17}
$$

The assumption is now made that the Leontovich[8] conditions for the application of the impedance boundary condition are satisfied. That is, the depth of penetration into the body and the wavelength in it are small in comparison to the free space wavelength, in comparison to the distances from the sources of the field, and in comparison to

the radii of curvature of the surface of the body. Hence the product $\mu\epsilon$ is complex and the imaginary part of $\sqrt{\epsilon\mu}$ is a large quantity. Under these conditions the boundary condition on the surface s is

$$\hat{n} \times \bar{E}^T = z_s\left(\hat{n} \times (\hat{n} \times \bar{H}^T)\right) , \tag{18}$$

where $z_s = \sqrt{\mu/\epsilon}$ is the intrinsic impedance of the scatterer.

$$z_s = \frac{|\hat{n} \times \bar{E}^T|}{|\hat{n} \times \hat{n} \times \bar{H}^T|} . \tag{19}$$

The absolute value in Eq. (19) is taken to mean the modulus of the vector, retaining the phasor nature of z_s. In other words, $z_s = \sqrt{\mu/\epsilon}$ may be complex.

From Eqs. (14), (15), (16), (17) and (19) then,

$$R_{||} = \frac{1 - \frac{z_o}{z_s} \sin\theta}{1 + \frac{z_o}{z_s} \sin\theta} , \tag{20}$$

and

$$R_{\perp} = -\left\{\frac{1 - \frac{z_s}{z_o} \sin\theta}{1 + \frac{z_s}{z_o} \sin\theta}\right\} , \tag{21}$$

which are the approximate Fresnel reflection coefficients.[8] Then,

$$\begin{aligned} \bar{E}^T \times \hat{n} = \{&\hat{x} \sin\phi \cos\phi \sin\theta [R_{\perp} - R_{||}] + \\ &\hat{y} \sin\theta [1 + R_{\perp} \sin^2\phi + R_{||} \cos^2\phi] + \\ &\hat{z} \cos\theta \sin\phi [1 + R_{\perp}]\} e^{jkz} , \end{aligned} \tag{22}$$

$$(23)\qquad \hat{n}\times\bar{H}^{T} = \{\hat{x}\sin\theta[1 - R_{\perp}\sin^{2}\phi - R_{\parallel}\cos^{2}\phi] + \hat{y}\sin\phi\cos\phi\sin\theta[R_{\perp} - R_{\parallel}] + \hat{z}\cos\theta\cos\phi[1 - R_{\parallel}]\}\frac{e^{jkz}}{z_{o}}\quad ,$$

If the far field is to be calculated in the H-plane or yz plane of Fig. 1, for $y \geq 0$

$$\hat{r} = \hat{y}\sin\beta - \hat{z}\cos\beta$$

$$(24)\qquad \bar{\rho} = \rho\{\hat{x}\sin\theta'\cos\phi + \hat{y}\sin\theta'\sin\phi + \hat{y}\cos\theta'\}.$$

Thus, since $\rho\cos\theta' = z$ and $\rho\sin\theta' = \alpha(z)$,

$$(25)\qquad \bar{\rho}\cdot\hat{r} = \alpha(z)\sin\phi\sin\beta - z\cos\beta\,,$$

and in the H-plane far-field calculations

$$(26)\qquad \hat{r}\times(\hat{n}\times\bar{H}^{T}) = \{\hat{x}(\sin\beta\cos\theta\cos\phi[1-R_{\parallel}] - \cos\beta\sin\theta\sin\phi\cos\phi[R_{\perp}-R_{\parallel}]) - \hat{y}\cos\beta\sin\theta\cdot(\cos^{2}\phi[1-R_{\parallel}]+\sin^{2}\phi[1-R_{\perp}]) - \hat{z}\sin\beta\sin\theta\cdot(\cos^{2}\phi[1-R_{\parallel}]+\sin^{2}\phi[1-R_{\perp}])\}\frac{e^{jkz}}{z_{o}}\quad .$$

In the r'', θ'', ϕ'' spherical coordinate system of Fig. 1 where $\beta = \pi - \theta''$ in the H-plane,

$$(27)\qquad \bar{H}^{s}_{\theta''} = \hat{\theta}''(-\cos\beta\ H^{s}_{y} - \sin\beta\ H^{s}_{z})\,.^{9}$$

Equation (27) is valid in the far field and the "front" half of the H-plane ($y \geq 0$).

From Eqs. (7), (22), (25), (26) and (27), the scattered magnetic field in the H-plane is obtained in the far field and for $y \geq 0$ as

$$(28)\quad H_{\theta''}^{s} \simeq \frac{jke^{jkr}}{4\pi r z_o}\left\{-\cos\beta \iint_s \sin\theta \left[\cos^2\phi(1+\tilde{R}_{\parallel}-\cos\beta(1-R_{\parallel}))+\right.\right.$$
$$\left.\sin^2\phi(1+R_{\perp}-\cos\beta(1-R_{\perp}))\right] e^{-jk[\alpha(z)\sin\phi\sin\beta-z(\cos\beta+1)]}ds$$
$$+\sin\beta \iint_s \left[-\cos\theta\sin\phi(1+\tilde{R}_{\perp})+\sin\beta\sin\theta(\cos^2\phi(1-R_{\parallel})+\right.$$
$$\left.\left.\sin^2\phi(1-R_{\perp}))\right] e^{-jk[\alpha(z)\sin\phi\sin\beta-z(\cos\beta+1)]}ds\right\}.$$

In the E-plane or xz plane of Fig. 1,

$$(29)\quad \hat{r} = \hat{x}\sin\beta - \hat{z}\cos\beta, \qquad x \geq 0$$
$$\bar{\rho} = \rho\{\hat{x}\sin\theta'\cos\phi+\hat{y}\sin\theta'\sin\phi+\hat{z}\cos\theta'\},$$

and

$$(30)\quad \bar{\rho}\cdot\hat{r} = \alpha(z)\cos\phi\sin\beta - z\cos\beta.$$

Using Eqs. (23) and (29),

$$(31)\quad \hat{r}\times(\hat{n}\times\bar{H}^{T}) = \left\{\hat{x}\cos\beta\sin\theta\sin\phi\cos\phi[R_{\perp}-R_{\parallel}]-\right.$$
$$\hat{y}[\cos\beta\sin\theta(\cos^2\phi[1-R_{\parallel}]+\sin^2\phi[1-R_{\perp}])$$
$$+\sin\beta\cos\theta\cos\phi[1-R_{\parallel}]]+\hat{z}\sin\beta\sin\theta\sin\phi\cos\phi\cdot$$
$$\left.[R_{\perp}-R_{\parallel}]\right\}\frac{e^{jkz}}{z_o}$$

Again in the r'', θ'', ϕ'' spherical coordinate system in the E-plane,[9]

$$\bar{H}^s_{\phi''} = \hat{\phi}''(-\sin\phi'' H^s_x + \cos\phi'' H^s_y) = \hat{\phi}'' H^s_y, \quad \text{for } x \geq 0. \tag{32}$$

From Eqs. (7), (22), (30), (31) and (32), the scattered magnetic field in the E-plane far field is obtained for $x \geq 0$ as,

$$H^s_{\phi''} = \frac{jke^{jkr}}{4\pi r z_o}\left\{\iint_s \cos^2\phi \sin\theta[1+R_{||}-\cos\beta(1-R_{||})] \cdot e^{-jk[\alpha(z)\cos\phi\sin\beta - z(\cos\beta+1)]}\, ds - \iint_s \sin^2\phi \sin\theta[\cos\beta(1-R_\perp)-(1+R_\perp)] \cdot e^{-jk[\alpha(z)\cos\phi\sin\beta - z(\cos\beta+1)]}\, ds - \sin\beta \iint \cos\theta\cos\phi[1-R_{||}] \cdot e^{-jk[\alpha(z)\cos\phi\sin\beta - z(\cos\beta+1)]}\, ds\right\}. \tag{33}$$

Equations (28) and (33) give the entire scattered magnetic field in two orthogonal planes, since, by symmetry, the other components vanish. Since $ds = \alpha(z)\sqrt{(\alpha'(z))^2 + 1}\; dz\, d\phi$ and the limits of integration on ϕ and z are 0 to 2π and 0 to ℓ' respectively, where $z = \ell'$ denotes the geometrical shadow boundary of the scatterer, the integrations on ϕ in Eqs. (28) and (33) may be performed without specifying $\alpha(z)$. From Eq. (28), there are the following forms of integrals on ϕ,

$$\int_0^{2\pi} \cos^2 \phi \, e^{-jkA \sin\phi} \, d\phi,$$

(34)
$$\int_0^{2\pi} \sin^2 \phi \, e^{-jkA \sin\phi} \, d\phi,$$

$$\int_0^{2\pi} \sin\phi \, e^{-jkA \sin\phi} \, d\phi \quad .$$

Using the expansion,[10]

(35)
$$e^{-jkA \sin\phi} = \sum_{n=-\infty}^{\infty} J_n(kA) e^{-jn\phi} \, ,$$

and assuming that the summations are uniformly convergent with respect to ϕ so that the order of integration and summation may be interchanged, there are obtained,

(36)
$$\int_0^{2\pi} \sin\phi \, e^{-jkA \sin\phi} \, d\phi = -j 2\pi J_1(kA) \, ,$$

(37)
$$\int_0^{2\pi} \cos^2 \phi \, e^{-jkA\sin\phi} d\phi = \pi J_0(kA) + \frac{\pi}{2} J_2(kA) + \frac{\pi}{2} J_{-2}(kA)$$

$$= 2\pi \frac{J_1(kA)}{kA} \, ,$$

(38)
$$\int_0^{2\pi} \sin^2 \phi \, e^{-jkA \sin\phi} d\phi = \pi J_0(kA) - \frac{\pi}{2} J_2(kA) - \frac{\pi}{2} J_{-2}(kA)$$

$$= 2\pi J_1'(kA) \, ,$$

and for the integrals on ϕ in Eq. (33),

$$\int_0^{2\pi} \cos\phi\, e^{-jkA\cos\phi} d\phi = -j\,2\pi\, J_1(kA) \quad , \tag{39}$$

$$\int_0^{2\pi} \cos^2\phi\, e^{-jkA\cos\phi} d\phi = \pi J_0(kA) - \frac{\pi}{2} J_2(kA) - \frac{\pi}{2} J_{-2}(kA), \tag{40}$$

$$= 2\pi\, J_1'(kA)$$

$$\int_0^{2\pi} \sin^2\phi\, e^{-jkA\cos\phi} d\phi = \pi J_0(kA) + \frac{\pi}{2} J_2(kA) + \frac{\pi}{2} J_{-2}(kA) \tag{41}$$

$$= \frac{2\pi J_1[kA]}{kA} \quad .$$

The scattering cross-section is defined[11] as,

$$\sigma = \lim_{r\to\infty} 4\pi r^2 \left| \frac{\bar{H}^s}{\bar{H}^i} \right|^2 \quad , \tag{42}$$

From Eqs. (28) and (42), using Eqs. (36), (37), and (38) and the definitions of $R_{\parallel}$ and $R_{\perp}$ from Eqs. (20) and (21), the bistatic scattering cross section in the H-plane is found as,

$$\sigma_{\text{H-plane}}(\beta) = 4\pi k^2 \left| \cos\beta \int_0^{\ell'} \alpha(z)\alpha'(z) \left[\frac{\sqrt{(\alpha'(z))^2+1} - \frac{z_o}{z_s}\alpha'(z)\cos\beta}{\sqrt{(\alpha'(z))^2+1} + \frac{z_o}{z_s}\alpha'(z)} \right]^N \right. \tag{43}$$

$$\left. \frac{J_1[k\alpha(z)\sin\beta]}{k\alpha(z)\sin\beta} e^{jkz(\cos\beta+1)} dz \right|$$

$$-\cos\beta \int_o^{\ell'} \alpha(z)\alpha'(z) \left[\frac{\frac{z_s}{z_o}\alpha'(z) - \cos\beta\sqrt{(\alpha'(z))^2+1}}{\sqrt{(\alpha'(z))^2+1} + \frac{z_s}{z_o}\alpha'(z)} \right] J_1'[k\alpha(z)\sin\beta] \cdot$$

$$\cdot e^{jkz(\cos\beta+1)}dz$$

$$+j\sin\beta \int_o^{\ell'} \frac{z_s \alpha(z)\alpha'(z)}{(z_o\sqrt{(\alpha'(z))^2+1} + z_s\alpha'(z))} J_1[k\alpha(z)\sin\beta] e^{jkz(\cos\beta+1)}dz$$

$$+\sin^2\beta \int_d^{\ell'} \frac{\alpha(z)(\alpha'(z))^2 z_o}{z_s\sqrt{(\alpha'(z))^2+1} + z_o\alpha'(z))} \frac{J_1[k\alpha(z)\sin\beta]}{k\alpha(z)\sin\beta} e^{jkz(\cos\beta+1)}dz$$

$$+\sin^2\beta \int_o^{\ell'} \frac{\alpha(z)\alpha'(z)z_o\sqrt{\alpha'(z)^2+1}}{z_o\sqrt{(\alpha'(z))^2+1} + z_s\alpha'(z)} J_1'[k\alpha(z)\sin\beta] e^{jkz(\cos\beta+1)}dz \Bigg|^2$$

And from Eqs. (33) and (42) using Eqs. (27), (39), (40) and (41), the bistatic scattering cross-section in the E-plane is,

$$(44) \quad \sigma_{\text{E-plane}}(\beta) = 4\pi k^2 \Bigg| \int_o^{\ell'} \alpha(z)\alpha'(z) \left[\frac{z_s\sqrt{(\alpha'(z))^2+1} - z_o\alpha'(z)\cos\beta}{z_s\sqrt{(\alpha'(z))^2+1} + z_o\alpha'(z)} \right] \cdot$$

$$\cdot J_1'[k\alpha(z)\sin\beta] e^{jkz(\cos\beta+1)}dz$$

$$-\int_o^{\ell'} \alpha(z)\alpha'(z) \left[\frac{\cos\beta\, z_o\sqrt{(\alpha'(z))^2+1} - z_s\alpha'(z)}{z_o\sqrt{(\alpha'(z))^2+1} + z_s\alpha'(z)} \right] \frac{J_1[k\alpha(z)\sin\beta]}{k\alpha(z)\sin\beta}$$

$$\cdot e^{jkz(\cos\beta+1)}dz$$

$$+j\sin\beta \int_o^{\ell'} \frac{z_o\alpha(z)\alpha'(z)}{(z_s\sqrt{(\alpha'(z))^2+1} + z_o\alpha'(z))} \cdot J_1[k\alpha(z)\sin\beta] e^{jkz(\cos\beta+1)}dz \Bigg|^2,$$

where the relations[12]

$$J_o(\rho) - J_2(\rho) = 2J_1'(\rho),$$

$$J_o(\rho) + J_2(\rho) = \frac{2J_1(\rho)}{\rho}, \tag{45}$$

have been used to simplify the expressions. Setting the bistatic angle to zero in either (43) or (44) gives the monostatic axial echo area under impedance boundary conditions as

$$\sigma(0) = \pi k^2 \left| \int_o^{\ell'} \alpha(z)\alpha'(z) \left[\frac{z_s\sqrt{(\alpha'(z))^2+1} - z_o\alpha'(z)}{z_s\sqrt{(\alpha'(z))^2+1} + z_o\alpha'(z)} \right] e^{j2kz}\, dz \right. \tag{46}$$

$$\left. - \int_o^{\ell'} \alpha(z)\alpha'(z) \left[\frac{z_o\sqrt{(\alpha'(z))^2+1} - z_s\alpha'(z)}{z_o\sqrt{(\alpha'(z))^2+1} + z_s\alpha'(z)} \right] e^{j2kz}\, dz \right|^2 .$$

If the target is perfectly conducting, $z_s = 0$, from Eq. (46) the axial echo area is found as,

$$\sigma_M(0) = 4\pi k^2 \left| \int_o^{\ell'} \alpha(z)\,\alpha'(z)\, e^{j2kz} dz \right|^2 , \tag{47}$$

which is identical with Adachi's[3] first order approximation, except for the integration limit.

From Eq. (43) with $z_s = 0$ the bistatic cross-section in the H-plane for a perfectly conducting target is obtained as,

$$(48)\qquad \sigma_M(\beta) = 4\pi k^2 \left| \int_0^{\ell'} \alpha(z)\alpha'(z) J_0[k\alpha(z)\sin\beta]\, e^{jkz(\cos\beta + 1)}\, dz \right|^2 .$$

H-plane

Similarly, from Eq. (43) the bistatic cross-section in the E-plane for a perfectly conducting target is,

$$(49)\qquad \sigma_M(\beta) = 4\pi k^2 \left| j\sin\beta \int_0^{\ell'} \alpha(z) J_1[k\alpha(z)\sin\beta]\, e^{jkz(\cos\beta+1)} dz \right.$$

E-plane

$$\left. -\cos\beta \int_0^{\ell} \alpha(z)\alpha(z) J_0[k\alpha(z)\sin\beta]\, e^{jkz(\cos\beta+1)} dz \right|^2 .$$

Now if the Adachi conditions[1] are applied to the target, requiring that the scatterer be long, thin, and have a sharp apex if semi-infinite or apices if finite, and that the slope of the scatterer along the z axis be reasonably small everywhere, then

$$(50)\qquad \begin{aligned} &\sin\theta \simeq \tan\theta = \alpha'(z) << 1 , \\ &\cos\theta \simeq 1 . \end{aligned}$$

In this case the physical optics currents are assumed to exist over the entire length of the scatterer (i.e., $\ell' \to \ell$), and from Eq. (43),

$$(51)\quad \underset{\text{H-plane}}{\sigma'(\beta)} = 4\pi k^2 \Bigg| -\cos\beta \int_0^{\ell} \alpha(z)\alpha'(z) \left[\frac{1-\alpha'(z)\,\frac{z_o}{z_s}\cos\beta}{1+\frac{z_o}{z_s}\,\alpha'(z)} \right] \frac{J_1[k\alpha(z)\sin\beta]}{k\alpha(z)\sin\beta}$$

$$\cdot\, e^{jkz(\cos\beta+1)}\, dz$$

$$-\cos\beta \int_0^{\ell} \alpha(z)\alpha'(z) \left[\frac{\frac{z_s}{z_o}\alpha'(z)-\cos\beta}{1+\frac{z_s}{z_o}\,\alpha'(z)} \right] J_1'[k\alpha(z)\sin\beta]\, e^{jkz(\cos\beta+1)}\, dz$$

$$+j\sin\beta \int_0^{\ell} \frac{\frac{z_s}{z_o}\alpha(z)\alpha'(z)}{1+\frac{z_s}{z_o}\,\alpha'(z)}\, J_1[k\alpha(z)\sin\beta]\, e^{jkz(\cos\beta+1)}\, dz$$

$$+\sin^2\beta \int_0^{\ell} \frac{\alpha(z)(\alpha'(z))^2\,\frac{z_o}{z_s}}{1+\frac{z_o}{z_s}\,\alpha'(z)}\, \frac{J_1[k\alpha(z)\sin\beta]}{k\alpha(z)\sin\beta}\, e^{jkz(\cos\beta+1)}\, dz$$

$$+\sin^2\beta \int_0^{\ell} \frac{\alpha(z)\alpha'(z)}{1+\frac{z_s}{z_o}\,\alpha'(z)}\, J_1'[k\alpha(z)\sin\beta]\, e^{jkz(\cos\beta+1)}\, dz \Bigg|^2 .$$

For the perfectly conducting long, thin body, $z_s = 0$,

$$(52)\quad \underset{\text{H-plane}}{\sigma_M'(\beta)} = 4\pi k^2 \left| \int_0^{\ell} \alpha(z)\alpha'(z) J_o[k\alpha(z)\sin\beta]\, e^{jkz(\cos\beta+1)}\, dz \right|^2 .$$

In the E-plane from Eq. (44),

$$(53)\quad \sigma'(\beta) = 4\pi k^2 \Bigg| \int_0^{\ell} \alpha(z)\alpha'(z) \left[\frac{1 - \frac{z_o}{z_s}\alpha'(z)\cos\beta}{1 + \frac{z_o}{z_s}\alpha'(z)} \right] J_1'[k\alpha(z)\sin\beta] \cdot e^{jkz(\cos\beta + 1)} dz$$

$$- \int_0^{\ell} \alpha(z)\alpha'(z) \left[\frac{\cos\beta - \frac{z_s}{z_o}\alpha'(z)}{1 + \frac{z_s}{z_o}\alpha'(z)} \right] \frac{J_1[k\alpha(z)\sin\beta]}{k\alpha(z)\sin\beta} e^{jkz(\cos\beta+1)} dz$$

$$+ j\sin\beta \int_0^{\ell} \frac{\frac{z_o}{z_s}\alpha(z)\alpha'(z)}{1 + \frac{z_o}{z_s}\alpha'(z)} J_1[k\alpha(z)\sin\beta] e^{jkz(\cos\beta+1)} dz \Bigg|^2 .$$

For the perfectly conducting target,

$$(54)\quad \sigma_M'(\beta) = 4\pi k^2 \Bigg| j\sin\beta \int_0^{\ell} \alpha(z) J_1[k\alpha(z)\sin\beta] e^{jkz(\cos\beta+1)} dz$$

$$\cos\beta \int_0^{\ell} \alpha(z)\alpha'(z) J_0[k\alpha(z)\sin\beta] e^{jkz(\cos\beta+1)} dz \Bigg|^2 .$$

From Eq. (45) the axial back scatter from a long thin target is,

$$(55)\quad \sigma'(0) = 4\pi k^2 \left[\frac{z_s}{z_o} - \frac{z_o}{z_s} \right]^2 \left| \int_0^{\ell} \frac{\alpha(z)(\alpha'(z))^2 e^{j2kz} dz}{(1 + \frac{z_o}{z_s}\alpha'(z))(1 + \frac{z_s}{z_o}\alpha'(z))} \right|^2 .$$

For a perfect conductor, from Eq. (55)

$$(56)\quad \sigma_M'(0) = 4\pi k^2 \left| \int_0^{\ell} \alpha(z)\alpha(z) e^{j2kz} dz \right|^2 .$$

The expression in Eq. (56) is the same as Adachi's[3] first order approximation.

The standard physical optics results for the H-plane, E-plane and monostatic cross-sections respectively are given by Eqs. (43), (44), and (46) for an arbitrary surface impedance, and by Eqs. (48), (49), and (47) for the perfectly conducting scatterer. The corresponding results for the long, thin targets, where it is assumed that the physical optics currents on the illuminated surface exist over the entire scatterer ($\ell^i \to \ell$), that the target has a sharp apex or apices, and that the slope along the z axis is reasonably small ($\sqrt{a'(z)^2+1} \simeq 1$), are given by Eqs. (51), (53) and (55) for an arbitrary surface impedance, and by Eqs. (52), (54), and (56) for the perfect conductor. These equations comprise the results necessary to apply the physical optics approximation to any general rotationally symmetric target with an arbitrary surface impedance and a modification of the physical optics approximation to a particular class of long, thin targets with an arbitrary surface impedance.

In the case of long, thin targets, where a modification of the physical optics approximation is used, three difficulties exist which must be eliminated, or at least rationalized, before proceeding to an application of the results. In the remainder of this section, it will be demonstrated that; (1) the assumption of the physical optics

currents on the shadow region of the scatterer removes the polarization dependence of the bistatic results for rotationally symmetric conducting targets. This will be proved in particular for Eqs. (52) and (54) (the E- and H-plane results for long, thin targets), and a general proof will also be given. (2) The accuracy of the forward scatter cross-section predicted by the long, thin target results is questionable, at least for realistic targets, and an alternative variational result is derived. (3) The Leontovich conditions[8] for the application of the impedance boundary condition cannot be satisfied at the apices of long, thin targets, and the contribution from these portions of the scatterer are in doubt. Further, it is apparent from the derived results in Eqs. (51), (53), and (55), the long, thin target cross-sections for an arbitrary surface impedance, that for finite scatterers particular combinations of impedance ratio (z_s/z_o), and target slope ($\alpha'(z)$) in the shadow region, will result in an enhancement of the cross-section over the corresponding result for the perfectly conducting target. This is demonstrated in Chapter III for the case of axial backscatter from symmetric double cones. No experimental evidence is available at present to either support or disprove this result, although backscatter enhancement has been demonstrated for a conducting circular ogive with an asymmetric absorber coating on the rear apex.[26]

The lack of polarization dependence in Eqs. (52) and (54) may be demonstrated as follows. In Eq. (52), using the relation[12]

$$(57) \qquad \frac{d}{dp}\left[p J_1(p)\right] = p J_0(p),$$

the integral may be written as

$$(58) \qquad I_1 = \frac{1}{k \sin\beta} \int_0^{\ell} \frac{d}{dz}\left\{\alpha(z) J_1[B\alpha(z)]\right\} e^{jkz(\cos\beta+1)} dz.$$

An integration by parts gives,

$$(59) \qquad I_1 = -j \frac{(\cos\beta+1)}{\sin\beta} \int_0^{\ell} \alpha(z) J_1[k\alpha(z)\sin\beta]\, e^{jkz(\cos\beta+1)} dz \ .$$

It may be seen by comparing Eqs. (52) and (54), that

$$(60) \qquad \underset{\text{E-plane}}{\sigma'_M(\beta)} = \underset{\text{H-plane}}{\sigma'_M(\beta)} \ .$$

This may be shown in general for rotationally symmetric targets as follows;* for a perfectly conducting target, the physical optics approximation gives the scattered E and H field (tangential components) as $E^s = -E^i$, $H^s = H^i$, over the illuminated portion of the scatterer, and as $E^s = -E^i$, $H^s = -H^i$ over the shadow portion. The extended

---

*The author is indebted to Dr. E.M. Kennaugh for this proof.

long, thin body approximation however gives (tangential components) $E^s = -E^i$, $H^s = H^i$ over the entire scatterer. Thus Eq. (1) becomes, for long, thin, shapes,

$$\bar{H}^s = \frac{2}{4\pi} \iint_s \nabla \times \left[\frac{e^{jkR}}{R} \hat{n} \times \bar{H}^i \right] ds \ .$$

Now Eq. (1) holds when the scattered fields or the scattered fields plus any fields whose sources are external to s are integrated. Using duality, and recalling that the physical optics scattered fields on the illuminated portion are assumed over the entire surface s, the incident field may be subtracted and there is obtained from Eq. (1),

$$\bar{E}^s = -\frac{2}{4\pi} \iint_s \nabla \times \left[\frac{e^{jkR}}{R} \hat{n} \times \bar{E}^i \right] ds. \tag{62}$$

Thus, if the H-plane scattering is calculated using Eq. (61) and the polarization of the incident fields is then changed by $\pi/2$, keeping the same direction of propagation, the E-plane scattering may be calculated using Eq. (62). Since E^i and H^i are related by $\sqrt{\mu/\epsilon}$ in the far field, the results from Eqs. (61) and (62) are seen to be identical. The general result may be stated then that if the scattered fields (E^s and H^s) are assumed to be the negative and positive respectively of the incident fields (E^i and H^i) over the entire scatterer surface, then the results using Eq. (1) in any two orthogonal planes are identical. Clearly, there is no way of deducing in general whether the

bistatic results are more valid in one plane than another or possibly are an average of the two orthogonal planes, and this question must be resolved by a comparison of the theory with experimental results. In the case of a sphere, Keller's geometrical theory of diffraction [25] predicts that a diffracted ray traveling around the sphere and thence to a receiver would be obtained in the E-plane but not in the H-plane. It might be reasoned from this result that the predicted scattering will correspond to the E-plane, but this type of deduction is not completely conclusive by any means. In Chapter IV it is shown that theoretical calculations using the long, thin target approximation do agree with E-plane experimental results.

A second obvious difficulty with the results of the modified integral formulation for long, thin targets is the cross-section predicted for forward scatter. If $\beta = \pi$ in Eqs. (51) or (53) then,

$$\sigma'(\pi) = 4\pi k^2 \left| \int_0^{\ell} \alpha(z)\, \alpha'(z)\, dz \right|^2 . \tag{63}$$

For finite scatterers where $\alpha(0) = \alpha(\ell) = 0$, an integration by parts yields

$$\sigma'(\pi) \equiv 0, \tag{64}$$

which is obviously in error, at least for realistic targets. The forward scattering cross-section for axial incidence from rotationally

symmetric, conducting, long, thin targets with apices may also be derived using a variational technique. From the results of Storer and Sevick,[13] the variational expression for the bistatic scattering cross-section is found to be,

$$(65)\qquad \sigma'_M(\beta) = \frac{k^2 z_o^2}{4\pi}\left| \frac{\iint_s \bar{E}^i_{\alpha,\rho}(r)\cdot \bar{J}_{\alpha',\rho'}(r')ds \iint_s \bar{E}^i_{\alpha',\rho'}(r')\cdot \bar{J}_{\alpha,\rho}(r)ds}{-\iint_s \bar{E}^s_{\alpha,\rho}(r)\cdot \bar{J}_{\alpha',\rho'}(r')ds} \right|^2 ,$$

where $\hat{\alpha}$ and $\hat{\rho}$ are unit vectors in the polarization and propagation directions, respectively. Thus $\bar{E}^i_{\alpha,\rho}(r)$ is an incident field polarized in the $\hat{\alpha}$ direction and propagating in the $\hat{\rho}$ direction, $E^s_{\alpha,\rho}(r)$ is the scattered field on the scatterer surface due to $\bar{E}^i_{\alpha,\rho}(r)$ and $J_{\alpha,\rho}(r)$ $J_{\alpha',\rho'}(r')$ are the surface currents induced on the scatterer by $\bar{E}^i_{\alpha,\rho}(r)$ and $\bar{E}^i_{\alpha',\rho'}(r')$, respectively. Let

$$(66)\qquad \begin{aligned} \hat{\alpha} &= \hat{\alpha}' = \hat{x} \\ \hat{\rho} &= \hat{z} \\ \hat{\rho}' &= -\hat{z} , \end{aligned}$$

then the physical optics currents are,

$$(67)\qquad \begin{aligned} J_{\alpha,\rho}(r) &= [\hat{\xi}\cos\phi - \hat{\phi}\sin\theta\sin\phi]e^{jkz} \\ J_{\alpha',\rho'}(r) &= [-\hat{\xi}\cos\phi + \hat{\phi}\sin\theta\sin\phi]e^{-jkz} . \end{aligned}$$

Using the surface scattered fields found by Adachi,[3]

$$\tilde{E}_\xi = \frac{jz_o}{2k}\{\alpha''(z) + j2k\alpha'(z)\}\cos\phi\, e^{jkz}$$

$$(68)\qquad E_\phi = \frac{-jz_o}{2k}\{\alpha'(z) + jk\alpha(z)\}\frac{\sin\phi}{\alpha(z)}\, e^{jkz}$$

$$E_\phi^* = -\frac{z_o}{2}\sin\phi\, e^{jkz}$$

(E_ϕ^* is the scattered electric field due to the equivalent magnetic current, $kz = -z_o \sin\phi\, e^{jkz}$.) Equation (64) gives

$$(69)\qquad \sigma(\pi) = 16\pi k^4 \left| \frac{\left[\int_o^\ell \alpha(z)\alpha'(z)\sqrt{\alpha'(z)^2+1}\, dz\right]^2}{\int_o^\ell \{\alpha''(z)+j2k\alpha'(z)\}\alpha(z)\sqrt{\alpha'(z)^2+1}\,dz + \int_o^\ell \alpha'(z)dz} \right|^2 .$$

For $\alpha'(z)^2 \ll 1$, and $\alpha(0) = \alpha(\ell) = 0$, an integration by parts again yields

$$(70)\qquad \sigma(\pi) \simeq 4\pi k^2 \left| \int_o^\ell \alpha'(z)\alpha'(z)dz \right|^2 \equiv 0.$$

When the approximation $\sqrt{\alpha'(z)^2 + 1} \simeq 1$ is assumed the deduction must be made that for very large bistatic angles the assumption of the physical optics currents on the shadow portion of the scatterer leads to scattering cross-sections which would only be valid if the scatterer approached a needle-like shape. If the currents are removed from

the shadow region, that is, if ℓ^i denotes the shadow boundary then

$$\bar{J}'_{\alpha;\rho}(r) = 0 \qquad z \geq \ell^i$$

(71)

$$J'_{\alpha;\rho}(r) = 0 \qquad z \leq \ell^i \quad ,$$

and there is obtained from Eq. (65),

$$(72) \qquad \sigma(\pi) = 16\pi k^4 \left| \frac{\int_0^{\ell^i} \alpha(z)\alpha'(z)\sqrt{\alpha'(z)^2+1}\,dz \int_{\ell^i}^{\ell} \alpha(z)\alpha'(z)\sqrt{\alpha'(z)^2+1}\,dz}{\int_{\ell^i}^{\ell} \{\alpha''(z)+j2k\alpha'(z)\}\alpha(z)\sqrt{\alpha'(z)^2+1}\,dz + \int_{\ell^i}^{\ell} \alpha''(z)dz} \right|^2 .$$

Now for $\alpha'(z) << 1$, an integration by parts yields,

$$(73) \qquad \sigma(\pi) \simeq 4\pi k^2 \left| \int_0^{\ell^i} \alpha(z)\alpha'(z)dz \right|^2 .$$

If $\alpha(\ell^i) = a$, then

$$(74) \qquad \frac{\sigma(\pi)}{\pi a^2} \simeq (ka)^2 .$$

In general, the forward scattered cross-section should be calculated from Eq. (72) (the variational expression using the standard physical optics currents and Adachi's expressions Eq. (68) for the scattered fields on the target surface) since this expression reduces, as a first order approximation, to the well accepted value $(ka)^2$ for the normalized cross-section. The zero forward scatter predicted,

as a first order approximation, when the physical optics currents are assumed over the entire sca er may not be incorrect in the sense that as the slope becomes very small ($\alpha'(z) \to 0$), the target becomes a needle which may not cast a shadow (and hence have zero total scatter), but for practical targets a non-zero result is more reasonable.

It should be noted that Eq. (74), the first order approximation of the variational solution, Eq. (72), is just the forward scattered cross-section predicted by the standard physical optics results in Eqs. (43) and (44). An examination of the standard physical optics results reveals further that the normalized forward scatter cross-section predicted is a constant $(k\alpha(\ell^i))^2$, independent of the surface impedance. This same result has been demonstrated for the exact solution of the scattering from spheres under the impedance boundary condition,[15] where it is shown that for large ka (sphere circumference in wavelengths), a plot of the normalized forward scatter cross-section vs ka approaches the value $(ka)^2$, independent of the surface impedance of the sphere.

Marcinkowski[16] has also shown in the case of diffraction by an absorbing half-plane that the forward scattered fields are relatively unaffected by the surface impedance.

One additional factor concerning the validity of this integral formulation for imperfectly conducting long, thin scatterers should

be considered. Clearly, targets with a sharp apex or apices can never satisfy the Leontovich conditions for applying approximate boundary conditions at these points. Hence, the axial echo area as calculated from Eq. (55) should contain a different tip contribution. However, for $\alpha(z) << 1$, Eq. (55) should suffice except for very low reflection shapes.

In summary, the results derived in this section should be utilized as follows:

a. The monostatic, E-plane, and H-plane cross-sections of general shapes are calculated from Eq. (46), (44), and (43), respectively.

b. For targets in the "long, thin" classification, the monostatic cross-sections are calculated from Eq. (55) and the E-plane cross-sections from Eq. (53) for bistatic angles less than the specular reflection angle. The forward scatter cross-section is given by Eq. (72).

CHAPTER III
AXIAL BACKSCATTER

A. Semi-Infinite Cones

A semi-infinite cone characterized by a surface impedance $z_s = \sqrt{\mu/\epsilon}$ is shown in Fig. 2. From the figure, $\alpha(z) = z \tan \theta_o$.

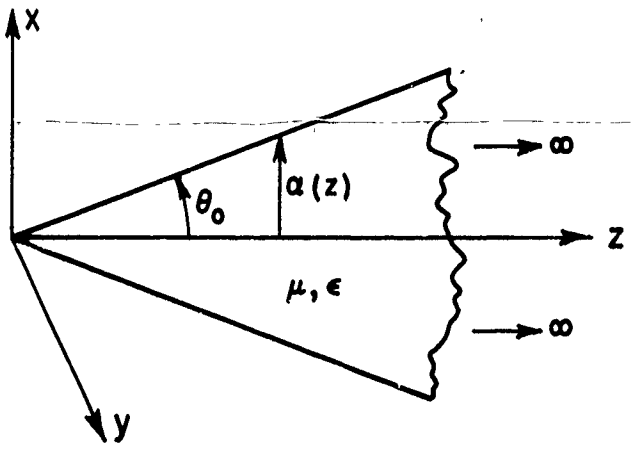

Fig. 2. Semi-infinite cone.

Using Eq. (46) and performing the integrations yields,

$$(75) \quad \frac{\sigma(0)}{\lambda^2} = \frac{\tan^6 \theta_o}{16\pi} \left[\frac{\sec \theta_o \{z_s^2 - z_o^2\}}{z_s z_o (1+2\tan^2 \theta_o) + (z_s^2 + z_o^2) \sec \theta_o \tan \theta_o} \right]^2 .$$

If θ_o is small such that the "long, thin" approximation applies, then from Eq. (55),

$$(76) \quad \frac{\sigma'(0)}{\lambda^2} = \frac{\tan^6 \theta_o}{16} \left[\frac{\frac{z_s}{z_c} - \frac{z_o}{z_s}}{1 + \tan^2 \theta_o + \tan \theta_o \left\{ \frac{z_s}{z_o} + \frac{z_o}{z_s} \right\}} \right]^2 .$$

Setting $z_s = 0$ in either Eq. (75) or Eq. (76) yields the physical optics approximation to a perfectly conducting semi-infinite cone as,

$$(77) \quad \frac{\sigma_M(0)}{\lambda^2} = \frac{\tan^4 \theta_o}{16\pi} \quad .$$

The axial echo area, as calculated from Eq. (76) for semi-infinite cones with half angles of 10, 20, 30, and 45 degrees as a function of the impedance ratio, z_s/z_o, is shown in Fig. 3. Note that a reciprocal impedance ratio scale is also given extending the range of this parameter from 1 to ∞. If should be noted that in Eqs. (46) and (55),

$$\sigma(0)\Big|_{\frac{z_s}{z_o} = \alpha} = \sigma(0)\Big|_{\frac{z_s}{z_o} = \frac{1}{\alpha}} \quad .$$

The axial echo area from a semi-infinite cone is the tip contribution discussed in Chapter II for a target with a sharp apex. Since, as was pointed out in Chapter II, the conditions for application of the impedance boundary condition are not satisfied at the tip, the reduction shown in Fig. 3 is an idealized case.

B. Double Cones

A double cone with the half angles θ_o and θ_1 is shown in Fig. 4.

$$(78) \quad \alpha(z) = \begin{cases} z \tan \theta_o & 0 \le z \le b, \\ -(z-c)\tan \theta_1 & b \le z \le c. \end{cases}$$

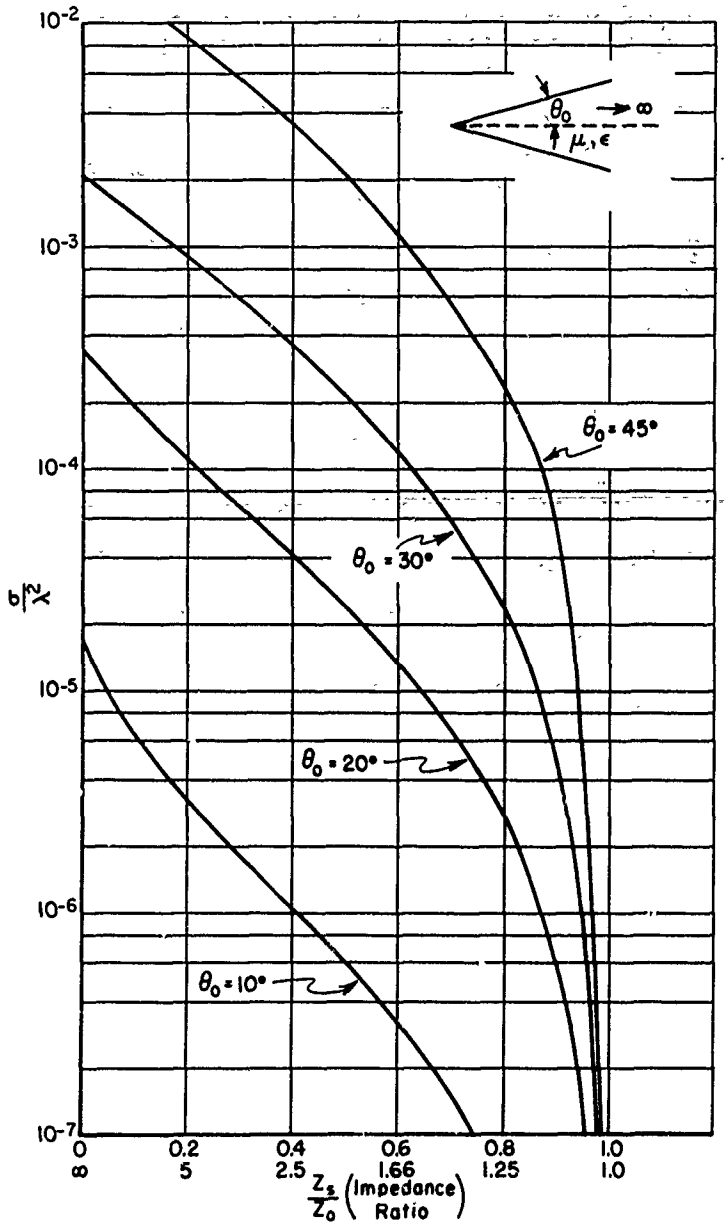

Fig. 3. Axial backscatter from semi-infinite cones as a function of the surface impedance.

From Eq. (55), the normalized axial echo area of a non-symmetric double cone is given by,

$$(79)\quad \frac{\sigma'(0)}{\pi a^2} = \frac{\tan^2\theta_o}{16(kb)^2}\left| C\{e^{j2kb}[1-j2kb]-1\} - D\frac{\tan^2\theta_1}{\tan^2\theta_o}\{e^{j2kb}[j2kc-j2kb+1]-e^{j2kc}\}\right|^2,$$

where,

$$C = \frac{1-\frac{z_o}{z_s}\tan\theta_o}{1+\frac{z_o}{z_s}\tan\theta_o} - \frac{1-\frac{z_s}{z_o}\tan\theta_o}{1+\frac{z_s}{z_o}\tan\theta_o}$$

$$D = \frac{1+\frac{z_o}{z_s}\tan\theta_1}{1-\frac{z_o}{z_s}\tan\theta_1} - \frac{1+\frac{z_s}{z_o}\tan\theta_1}{1-\frac{z_s}{z_o}\tan\theta_1}$$

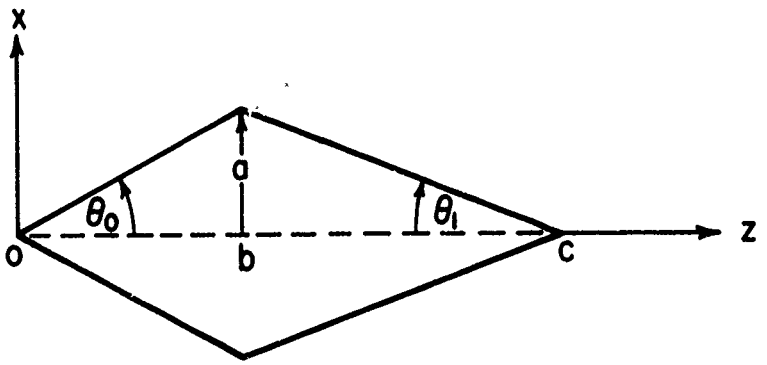

Fig. 4. Double cone.

The normalized axial echo areas from a $\theta_o = 10^o$ half angle double cone with $\tan\theta_1 / \tan\theta_o = 1.71234$, as a function of kb for z_s/z_o ratios of 0, .25, .5, and .75 are shown in Fig. 5.

Setting $\theta_1 = \theta_o$ and $c = 2b$ in Eq. (79) yields the normalized axial echo area of a symmetric double cone as,

$$(80) \quad \frac{\sigma'(0)}{\pi a^2} = \frac{\tan^2\theta}{16(kb)^2} \left| \begin{array}{l} C\{e^{j2kb}[1-j2kb]-1\} - \\ D^*\{e^{j2kb}[j2kb+1]-e^{j4kb}\} \end{array} \right|^2$$

$$D^* = \frac{1+\frac{z_o}{z_s}\tan\theta_o}{1-\frac{z_o}{z_s}\tan\theta_o} - \frac{1+\frac{z_s}{z_o}\tan\theta_o}{1-\frac{z_s}{z_o}\tan\theta_o} \quad .$$

The normalized axial echo areas of 10^o, 20^o, and 30^o half angle double cones as functions of the electrical length kb for z_s/z_o ratios of 0, .25, .5, and .75 are given in Figs. 6, 7, 8, 9, 10, and 11. In Figs. 6, 7, and 8, the cone half angle is the parameter, and in Figs. 9, 10, and 11 the ratio z_s/z_o is the parameter.

From Eq. (80), the high and low frequency limits are given by,

$$(81) \quad \frac{\sigma'(0)}{\pi a^2}_{kb\to\infty} = \frac{\tan^2\theta_o}{4}[C+D]^2$$

$$\frac{\sigma'(0)}{\pi a^2}_{kb\to 0} = \frac{\tan^2\theta_o}{16(kb)^2}\left|C\left[2(kb)^2+j\frac{8(kb)^3}{3}\right]-D^*\left[2(kb)^2+j\frac{16(kb)^3}{3}\right]\right|^2.$$

The measured[22] and theoretical axial backscatter from conducting double cones as calculated from Eq. (56) are compared in Fig. 12.

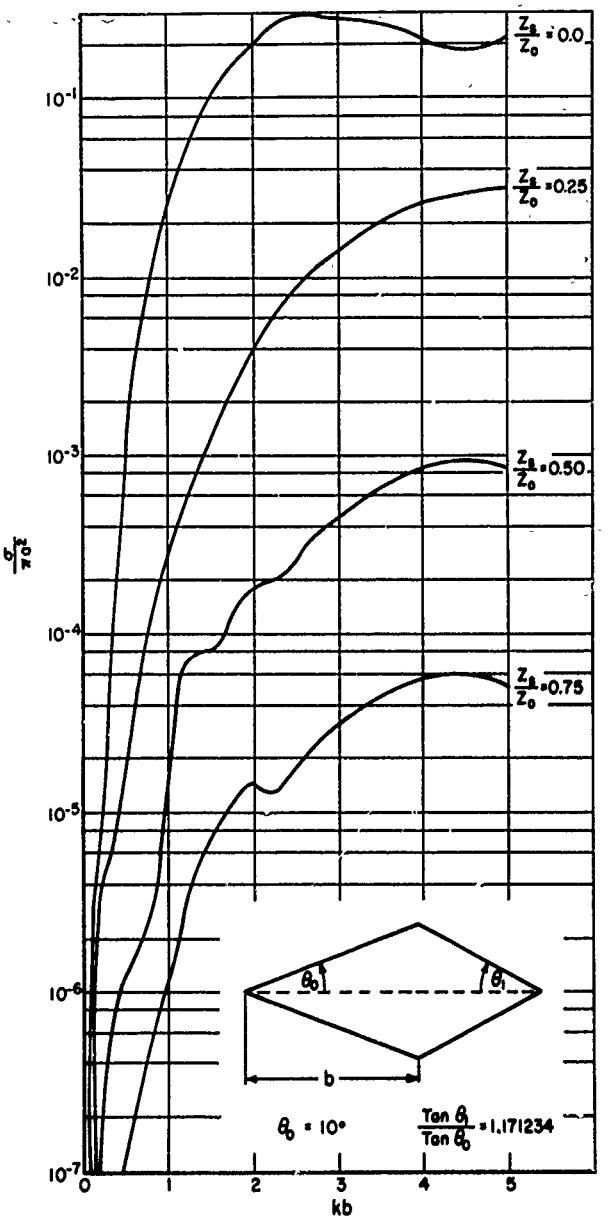

Fig. 5. Normalized axial backscatter from a nonsymmetric double cone. $\theta_0 = 10$ degrees, $\tan \theta_1 / \tan \theta_0 = 1.171234$.

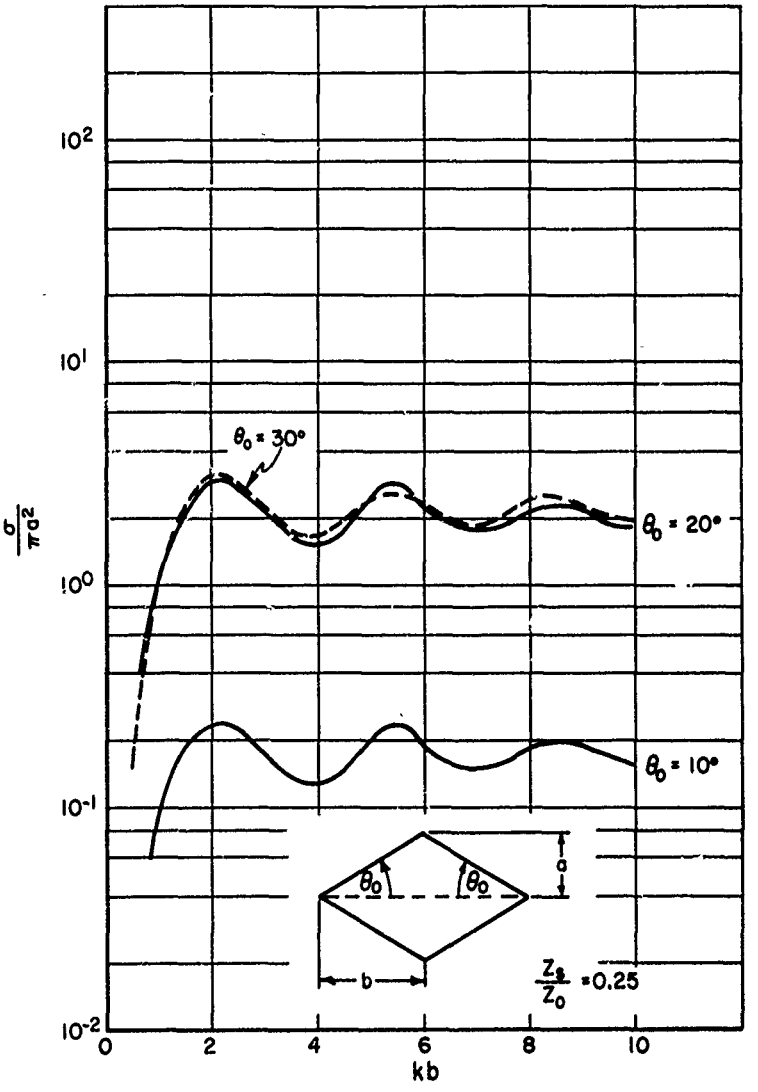

Fig. 6. Normalized axial backscatter from symmetric double cones for a surface to free space impedance ratio of .25.

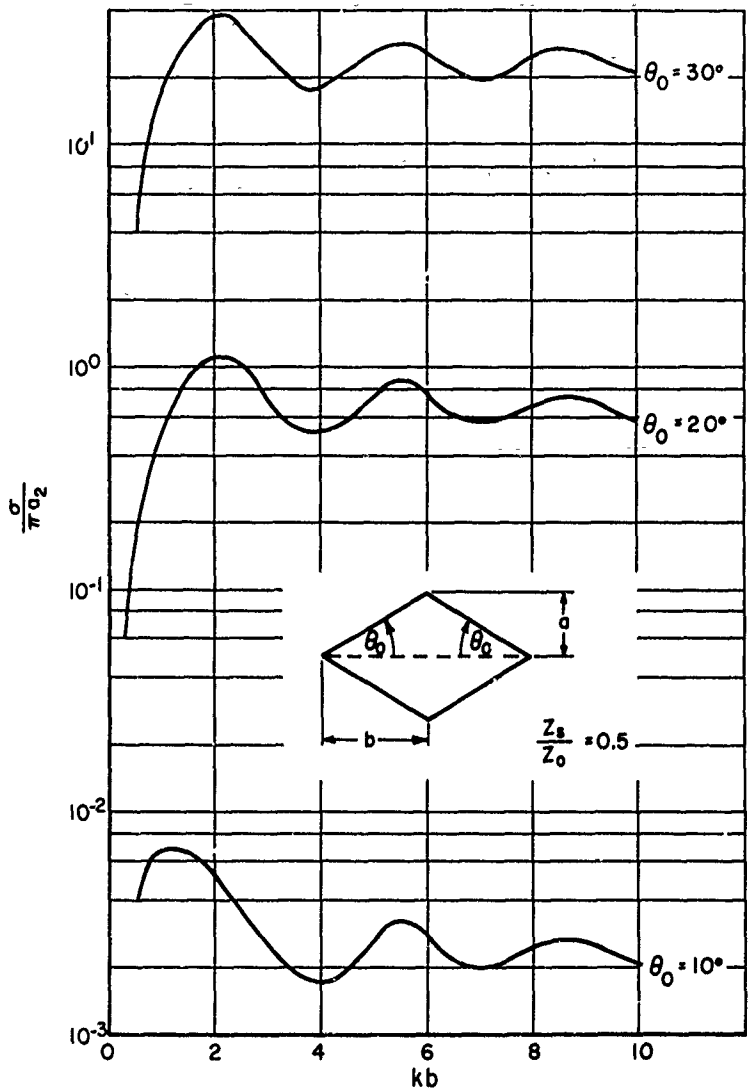

Fig. 7. Normalized axial backscatter from symmetric double cones for a surface to free space impedance ratio of .5.

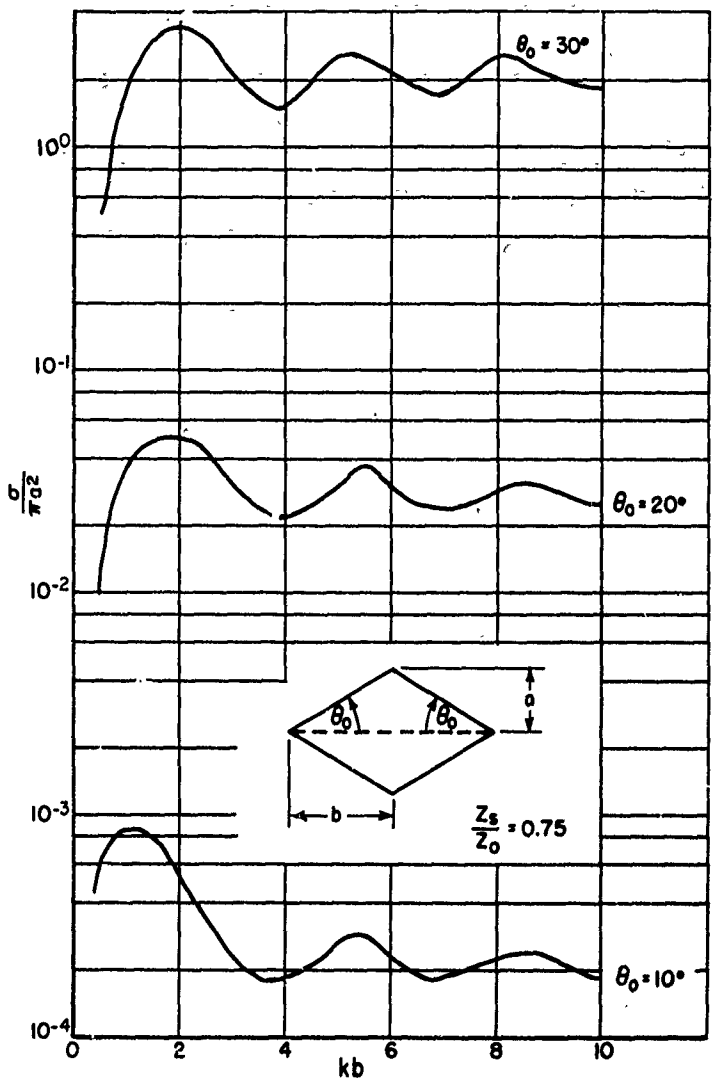

Fig. 8. Normalized axial backscatter from symmetric double cones for a surface to free space impedance ratio of .75.

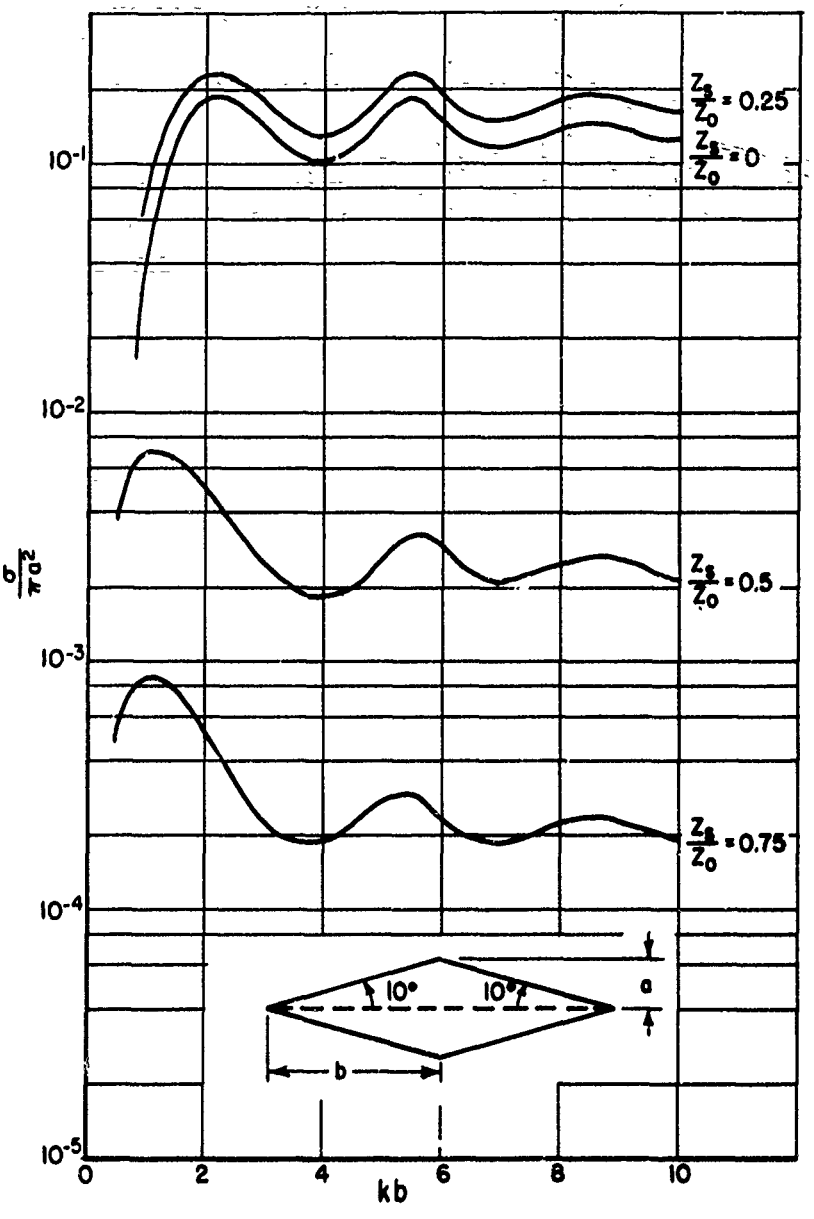

Fig. 9. Normalized axial backscatter from a 10 degree half angle symmetric double cone.

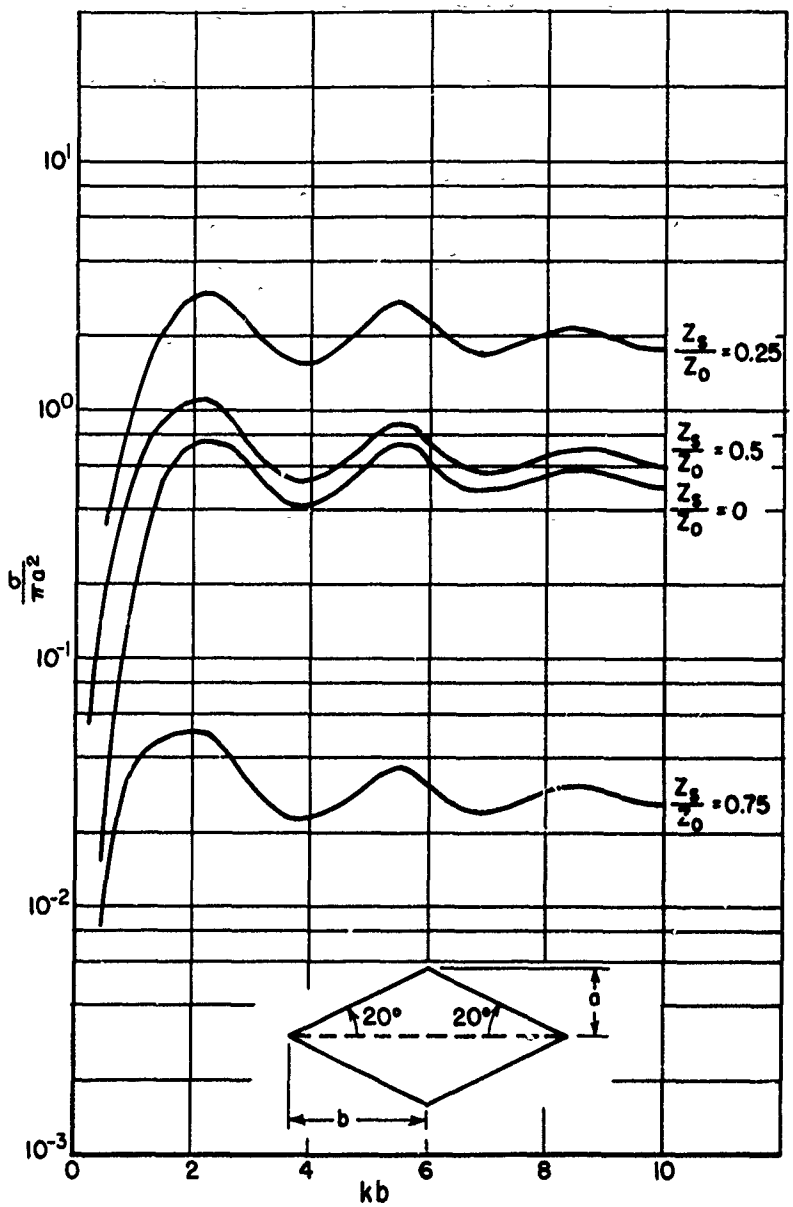

Fig. 10. Normalized axial backscatter from a 20 degree half angle symmetric double cone.

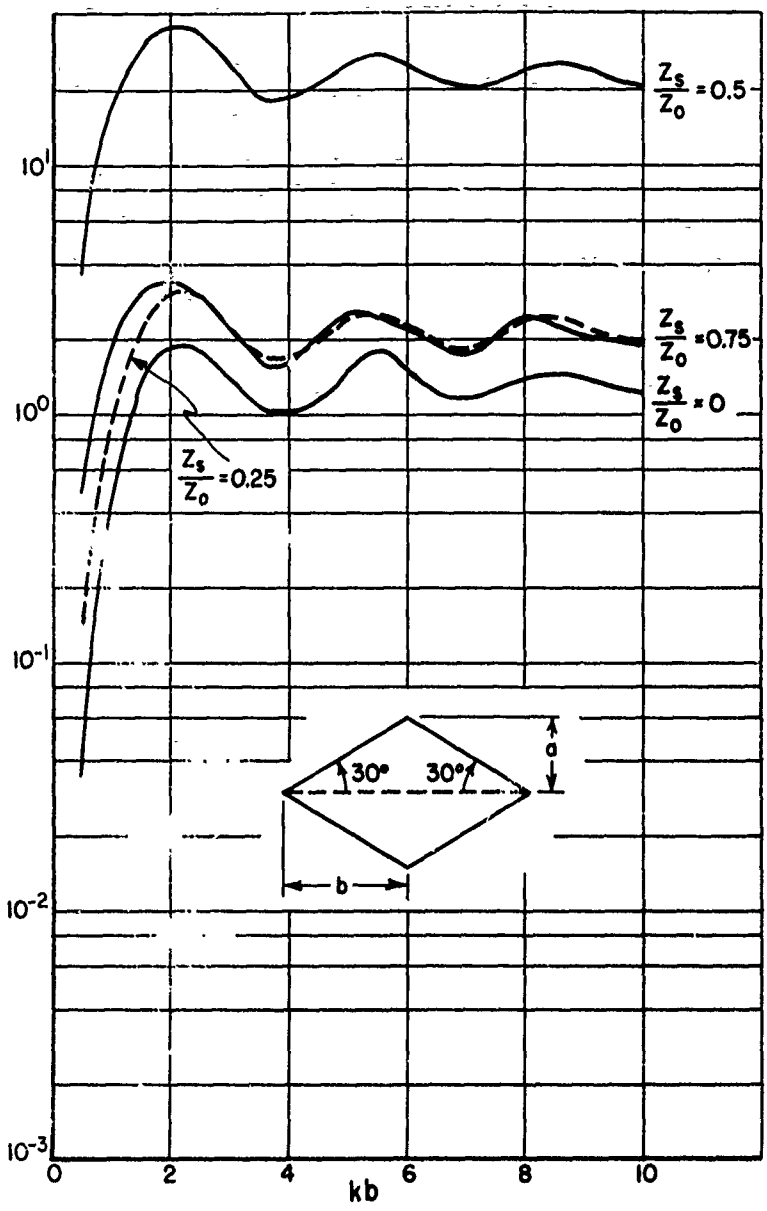

Fig. 11. Normalized axial backscatter from a 30 degree half angle symmetric double cone.

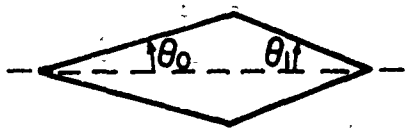

Cone		Measured		Theoreticai
θ_0	θ_1	H.P.	V.P.	
30	10	-2.0	-2.7	-2.36
30	20	-1.8	-0.5	+1.42
30	30	+0.5	+1.0	+0.68
20	10	-4.0	-4.0	-4.07
20	20	0.0	-1.0	-1.10
20	30	-1.5	-0.3	+1.42
10	10	-9.0	-8.5	-7.60
10	20	-5.0	-4.5	-4.07
10	30	-2.5	-2.7	-2.36

H.P. Horizontal Polarization
V.P. Vertical Polarization

Fig. 12. Measured and calculated axial backscatter from symmetric and nonsymmetric double cones.

C. Semi-infinite Cylinders with Conical Caps

Setting $\theta_1 = 0$ in Eq. (79) gives the normalized axial echo area of the semi-infinite cylinder capped with a cone of half angle θ_o shown in Fig. 13 as

$$(82) \quad \frac{\sigma'(0)}{\pi a^2} = \frac{\tan^2 \theta_o}{16(kb)^2} C^2 \left| e^{j2kb}[1-j2kb] - 1 \right|^2 .$$

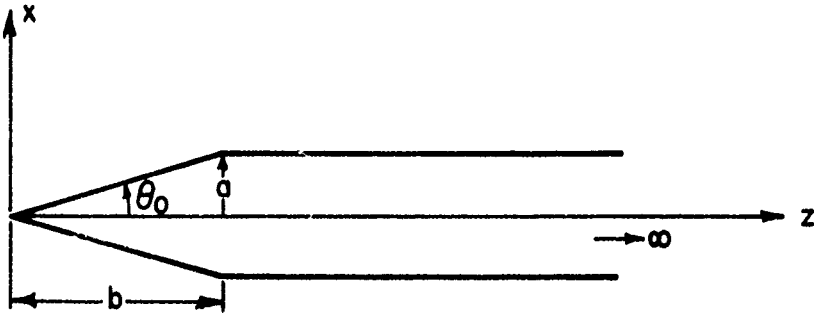

Fig. 13. Semi-infinite cylinder capped by a cone.

The normalized axial echo area of a semi-infinite cylinder of radius a capped with cones of half angles 10°, 20°, and 30° as a function of kb is shown in Figs. 14, 15, 16, 17, 18, and 19. In Figs. 14, 15, and 16, the half cone angle is the parameter, and in Figs. 17, 18, and 19, the impedance ratio z_s/z_o is the parameter.

The high and low frequency limits are given by

$$(83) \quad \frac{\sigma'(0)}{\pi a^2}_{kb \to \infty} = \frac{C^2 \tan^2 \theta_o}{4}$$

$$\frac{\sigma'(0)}{\pi a^2}_{kb \to 0} = \frac{\tan^2 \theta_o C^2 (kb)^2}{4} .$$

It is interesting to note that the result in Eq. (82) is generally attributed to the physical optics approximation for a finite, flat based cone. That is, Eq. (46) would give the same result as Eq. (82) for any target whose illuminated surface was a cone. Clearly in the limit as $k\nu \to \infty$, where ν is the illuminated length in the direction of the incident field, the axial echo area of rotationally symmetric targets becomes independent of the target shape in the shadow region. Hence, if $k\nu$ does not $\to \infty$ the results as given by Eq. (45), should be considered to be those for semi-infinite cylinders capped by various shapes.

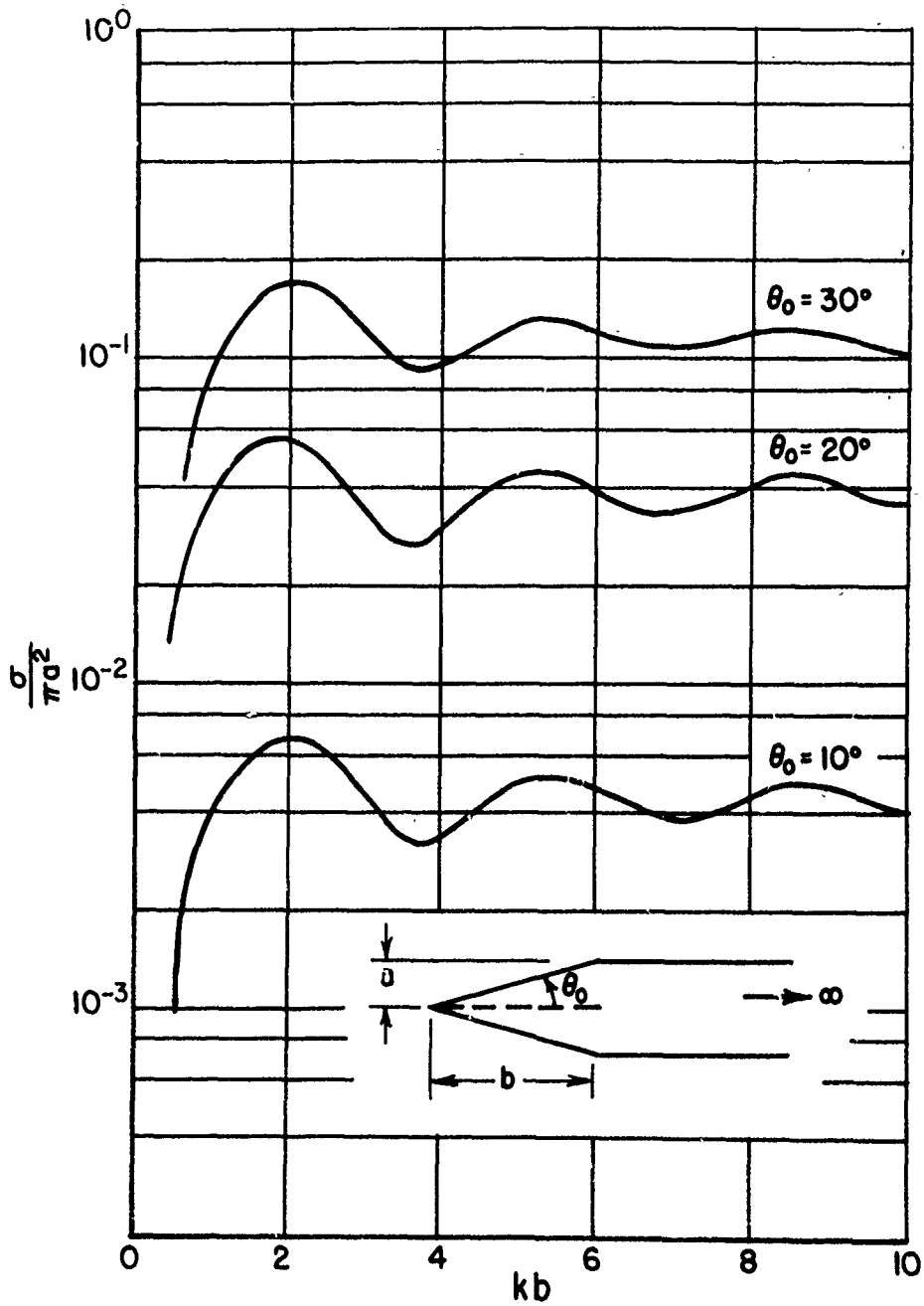

Fig. 14. Normalized axial backscatter from a semi-infinite cylinder of radius a capped by a cone for a surface to free space impedance ratio of .25.

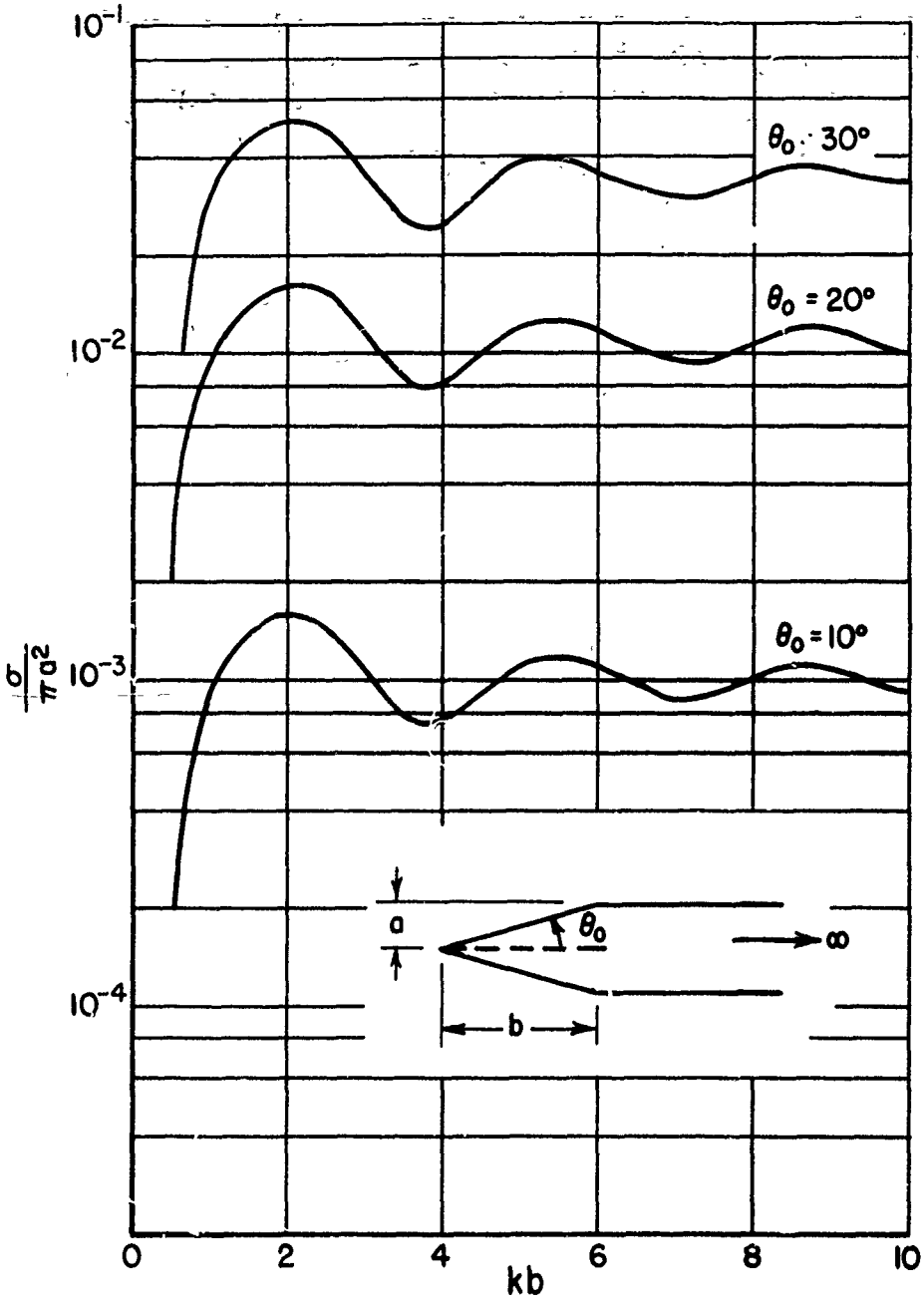

Fig. 15. Normalized axial backscatter from a semi-infinite cylinder of radius a capped by a cone for a surface to free space impedance ratio of .5.

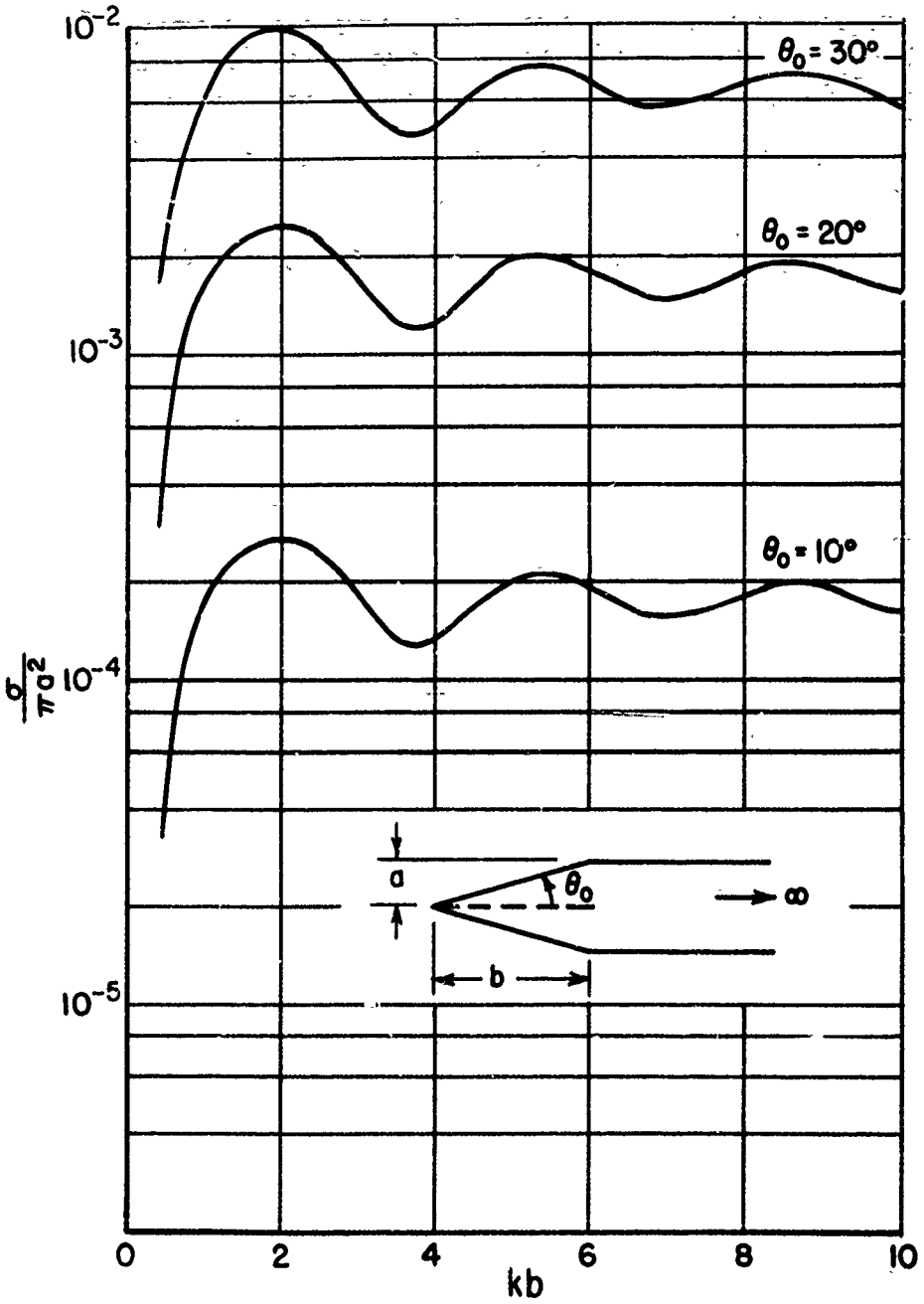

Fig. 16. Normalized axial backscatter from a semi-infinite cylinder of radius a capped by a cone for a surface to free space impedance ratio of .75.

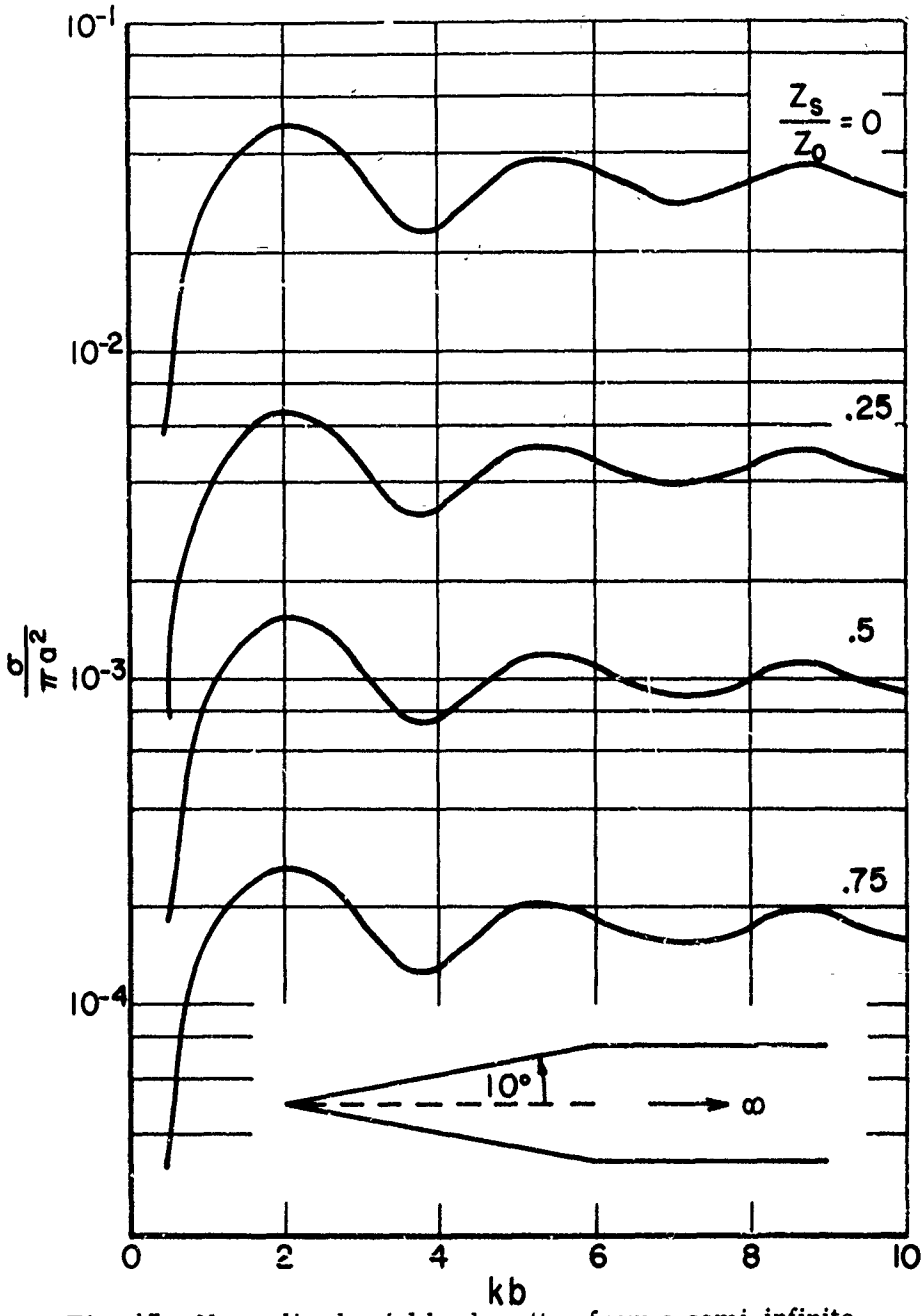

Fig. 17. Normalized axial backscatter from a semi-infinite cylinder of radius a capped by a 10 degree half angle cone.

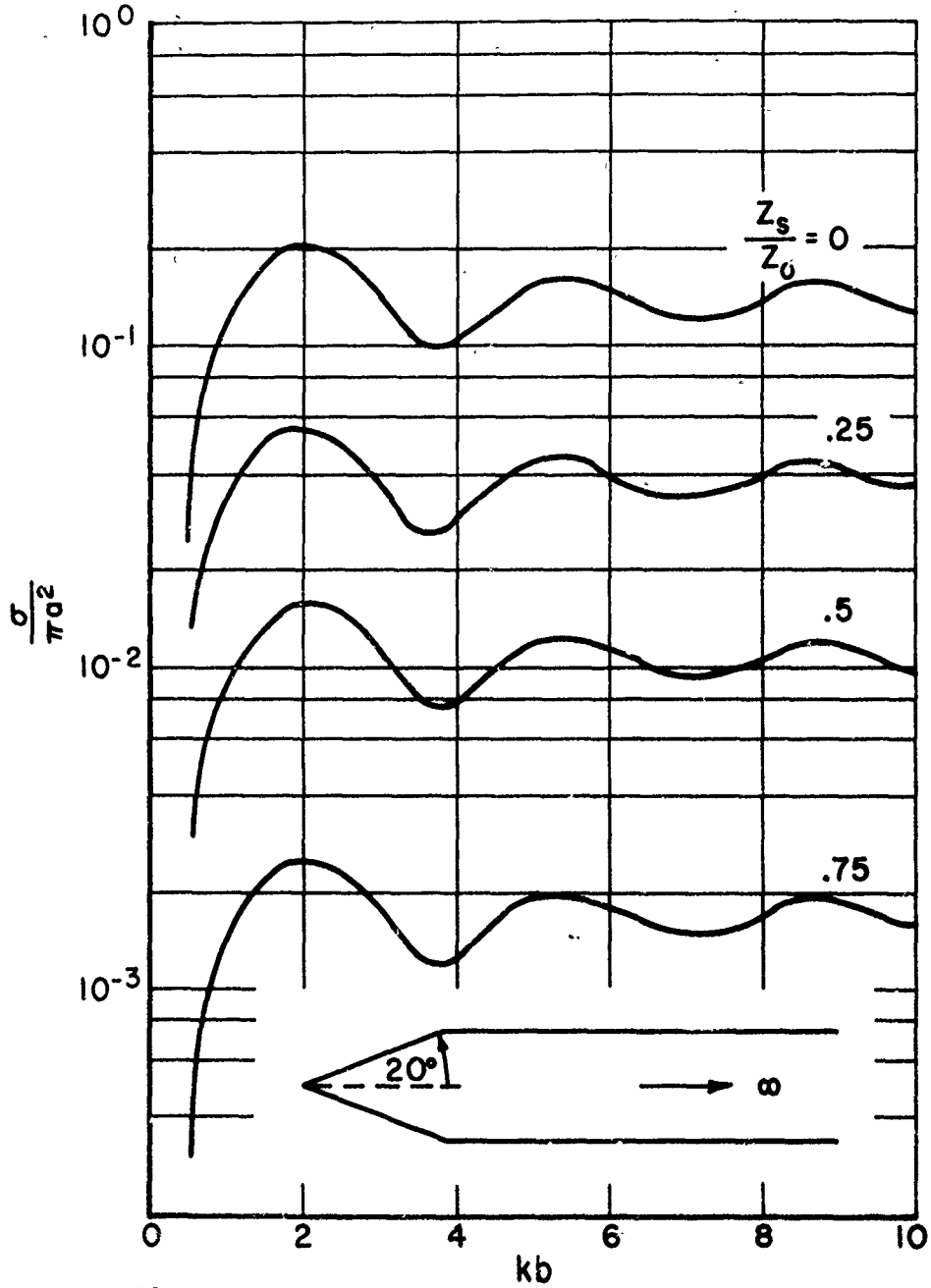

Fig. 18. Normalized axial backscatter from a semi-infinite cylinder of radius a capped by a 20 degree half angle cone.

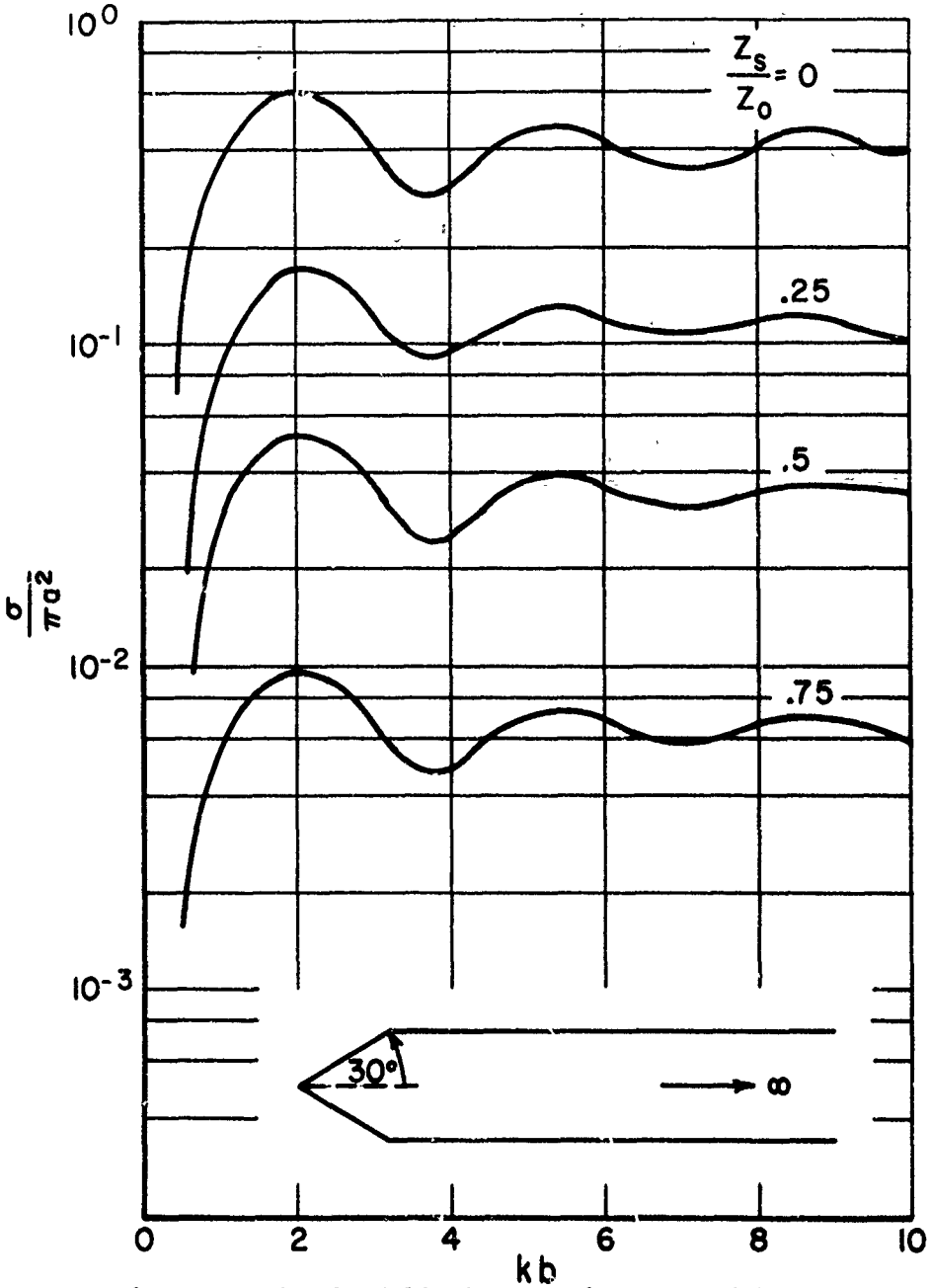

Fig. 19. Normalized axial backscatter from a semi-infinite cylinder of radius a capped by a 30 degree half angle cone.

D. Parabolic Ogive

A parabolic ogive is shown in Fig. 20.

$$(84)\quad \alpha(z) = a - \frac{a}{b^2}(z-b)^2 \ .$$

From Eq. (55), for $1/\tan\theta_o > z_s/z_o > \tan\theta_o$, the axial echo area is given by,

$$(85)\quad \frac{\sigma'(0)}{\lambda^2} = \frac{\tan^4\theta_o}{4\pi}\Bigg[\Big\{X\sin(2kb)\cos(2kb) - Y\sin^2(2kb) + Z\cos^2(2kb) + Q\{\cos\alpha(Ci(\alpha)-Ci(\alpha')+\sin\alpha(si(\alpha)-si(\alpha')\} + R\{\cos\beta(Ci(\beta)-Ci(\beta))+\sin\beta(si(\beta)-si(\beta)\}\Big\}^2 + \Big\{(Y+Z)\sin(2kb)\cos(2kb)+(X-T)\sin^2(2kb)-T\cos^2(2kb) + Q\{\sin\alpha(Ci(\alpha)-Ci(\alpha'))-\cos\alpha(si(\alpha)-si(\alpha'))\} + R\{\sin\beta(Ci(\beta)-Ci(\beta'))-\cos\beta(si(\beta)-si(\beta'))\}\Big\}^2\Bigg] \ ,$$

where

$$\alpha = 2k(A+b), \quad \alpha' = 2k(A-b)$$

$$\beta = 2k(B+b), \quad \beta' = 2k(B-b)$$

$$A = \frac{z_o}{z_s}\frac{b^2}{2a}, \quad B = \frac{z_s}{z_o}\frac{b^2}{2a}, \quad Ci(x) = -\int_x^\infty \frac{\cos t}{t}\,dt, \quad si(x) = -\int_x^\infty \frac{\sin t}{t}\,dt$$

$$X = \frac{kb}{\tan^3\theta_o}\left\{\left(\frac{z_o}{z_s}\right)^3 - \left(\frac{z_s}{z_o}\right)^3\right\} - \frac{1}{4ka}\left\{\frac{z_o}{z_s} - \frac{z_s}{z_o}\right\} + \frac{kb}{\tan^2\theta_o}\left\{\left(\frac{z_o}{z_s}\right)^2 - \left(\frac{z_s}{z_o}\right)^2\right\}$$

$$Y = \frac{1}{2\tan^2\theta_o}\left[\left(\frac{z_o}{z_s}\right)^2 - \left(\frac{z_s}{z_o}\right)^2\right]$$

$$Z = \frac{1}{\tan\theta_o}\left(\frac{z_o}{z_s} - \frac{z_s}{z_o}\right), \quad T = \frac{kb}{\tan^2\theta_o}\left\{\left(\frac{z_o}{z_s}\right)^2 - \left(\frac{z_s}{z_o}\right)^2\right\}$$

$$Q = \left(\frac{kb}{\tan\theta_o}\ \frac{z_o}{z_s}\right)^2\left(1 - \frac{(z_o/z_s)^2}{\tan^2\theta_o}\right), \quad R = \left(\frac{kb}{\tan\theta_o}\frac{z_s}{z_o}\right)^2\left(\frac{(z_s/z_o)^2}{\tan^2\theta_o} - 1\right)$$

$$\theta_o = \frac{2a}{b} \quad .$$

The normalized axial echo areas of a slender parabolic ogive with impedance ratios, z_s/z_o, of 0, and 0.5, are shown in Figs. 21 and 22. Now[17] for $x >> 1$,

$$\text{Ci}(x) \simeq \frac{\sin(x)}{x}$$

(86)

$$\text{si}(x) \simeq -\frac{\cos x}{x} \quad ,$$

and in the limit as $kb \to \infty$, for $1/\tan\theta_o > z_s/z_o > \tan\theta_o$,

$$(87) \quad \frac{\sigma'(0)}{\lambda^2} \xrightarrow[kb\to\infty]{} \frac{\tan^4\theta_o}{2\pi}\left[\left\{\left(\frac{z_o}{z_s}\right)^2 - \left(\frac{z_s}{z_o}\right)^2\right\}^2 \frac{1}{16\tan^4\theta_o}(1-\cos 4kb) + \left\{\frac{z_o}{z_s} - \frac{z_s}{z_o}\right\}^2 \frac{1}{4\tan^2\theta_o}(1+\cos 4kb)\right] .$$

It is of interest to note that when the slope of the scatterer profile is a function of z, the periodicity of the backscatter with kb is a function of both kb and the surface impedance.

E. Sphere

A sphere of radius a is shown in Fig. 23. From the figure,

$$(88) \qquad \alpha(z) = [2az - z^2]^{\frac{1}{2}} .$$

From Eq. (46) the normalized echo area is given by,

$$(89) \qquad \frac{\sigma}{\pi a^2} = 4(ka)^2 \left\{ \left[\left(\frac{z_s}{z_o} - \frac{z_o}{z_s} \right) \frac{\sin(2ka)}{2ka} - \frac{z_s^2}{z_o^2}(AC+BD) + \frac{z_o^2}{z_s^2}(A'C'+B'D') \right]^2 \right.$$

$$+ \left[\left(\frac{z_s}{z_o} - \frac{z_o}{z_s} \right) \frac{1}{2ka} + \left(\frac{z_o}{z_s} - \frac{z_s}{z_o} \right) \frac{\cos(2ka)}{2ka} - \frac{z_s^2}{z_o^2}(BC-AD) \right.$$

$$\left. \left. + \frac{z_o^2}{z_s^2}(B'C' - A'D') \right]^2 \right\} ,$$

where

$$A = \cos\left[2ka \left(1 + \frac{z_s}{z_o} \right) \right] , \qquad A' = \cos\left[2ka \left(1 + \frac{z_o}{z_s} \right) \right]$$

$$B = \sin\left[2ka \left(1 + \frac{z_s}{z_o} \right) \right] , \qquad B' = \sin\left[2ka \left(1 + \frac{z_o}{z_s} \right) \right]$$

$$C = \left[Ci\left[2ka \left(1 + \frac{z_s}{z_o} \right) \right] - Ci\left[2ka \frac{z_s}{z_o} \right] \right]$$

$$C' = \left[Ci\left[2ka \left(1 + \frac{z_o}{z_s} \right) \right] - Ci\left[2ka \frac{z_o}{z_s} \right] \right]$$

$$D = \left[si\left[2ka \left(1 + \frac{z_s}{z_o} \right) \right] - si\left[2ka \frac{z_s}{z_o} \right] \right]$$

$$D' = \left[si\left[2ka \left(1 + \frac{z_o}{z_s} \right) \right] - si\left[2ka \frac{z_o}{z_s} \right] \right].$$

The echo areas as functions of ka for impedance ratios, z_s/z_o, of 1.5 and 2 are shown in Figs. 24 and 25. The Mie series solutions under impedance boundary conditions[15] are included in the figures. In the limit as ka $\to \infty$,

$$(90) \quad \frac{\sigma}{\pi a^2} \quad ka \to \infty \quad \left(\frac{z_s - z_o}{z_s + z_o} \right)^2 ,$$

Eq. (90) is merely the square of the infinite plane reflection coefficient for normal incidence.

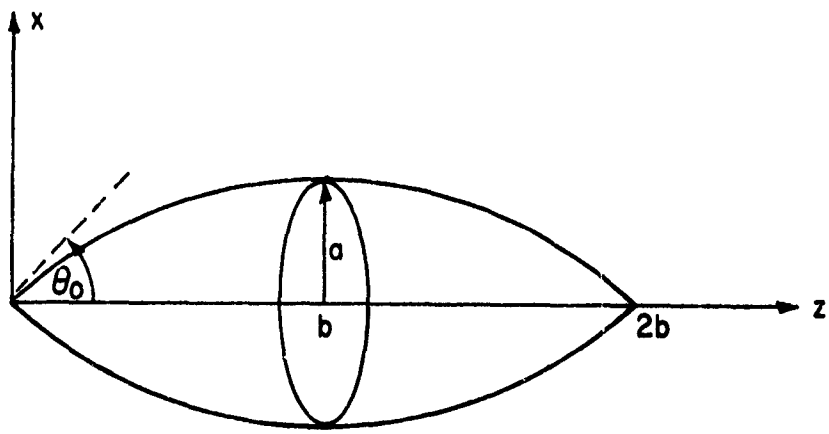

Fig. 20. Parabolic ogive.

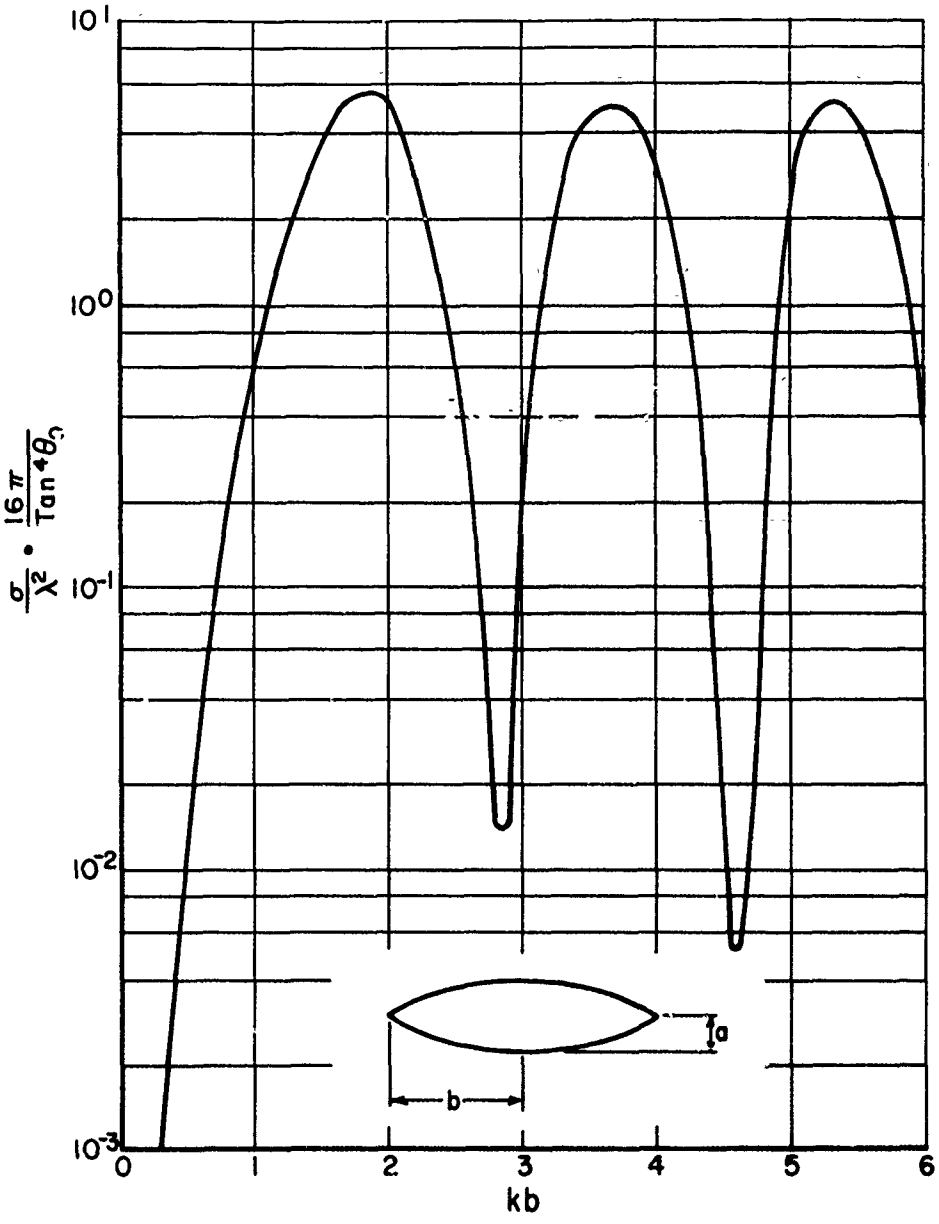

Fig. 21. Normalized axial backscatter from a parabolic ogive for surface to free space impedance ratio of 0.

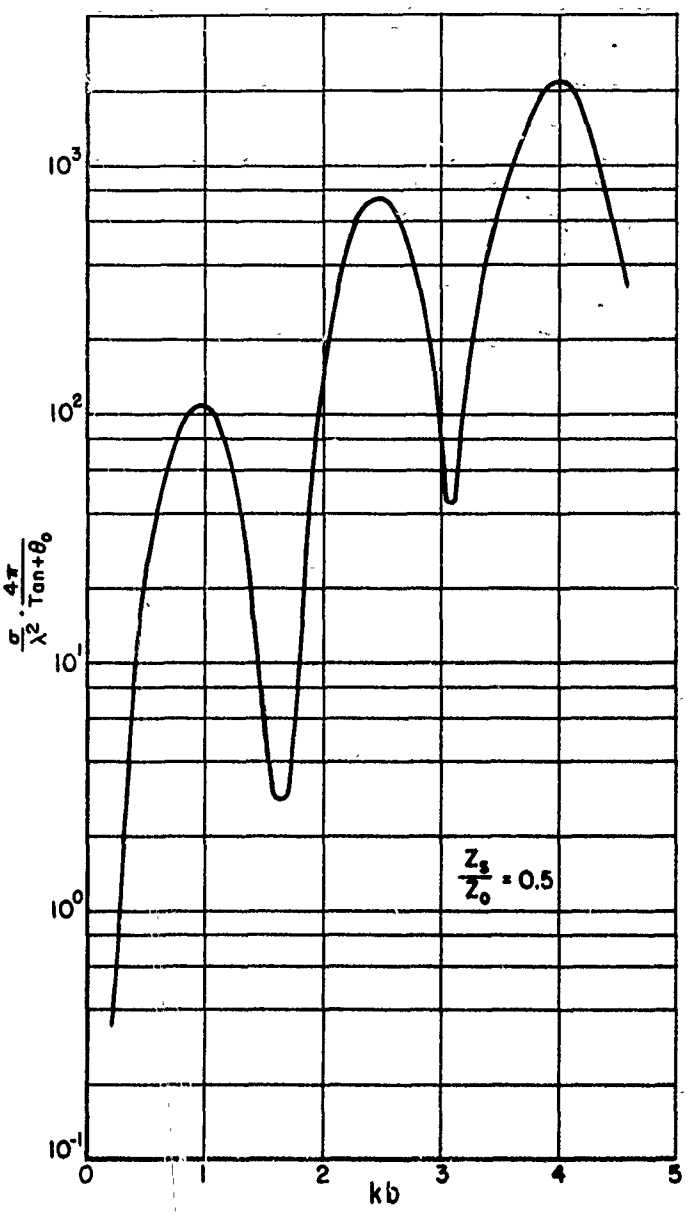

Fig. 22. Normalized axial backscatter from a parabolic ogive for surface to free space impedance ratio of 0.5.

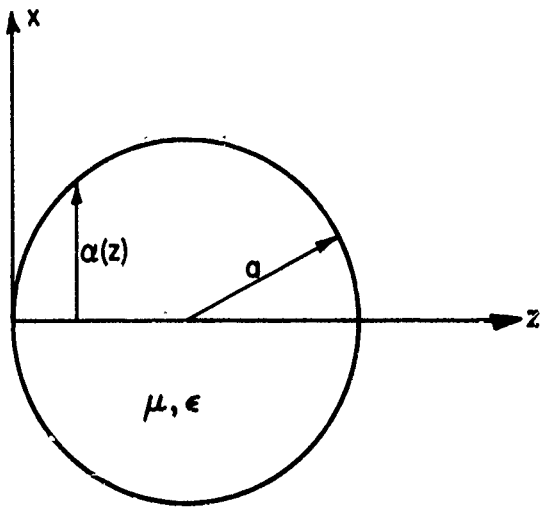

Fig. 23. Sphere.

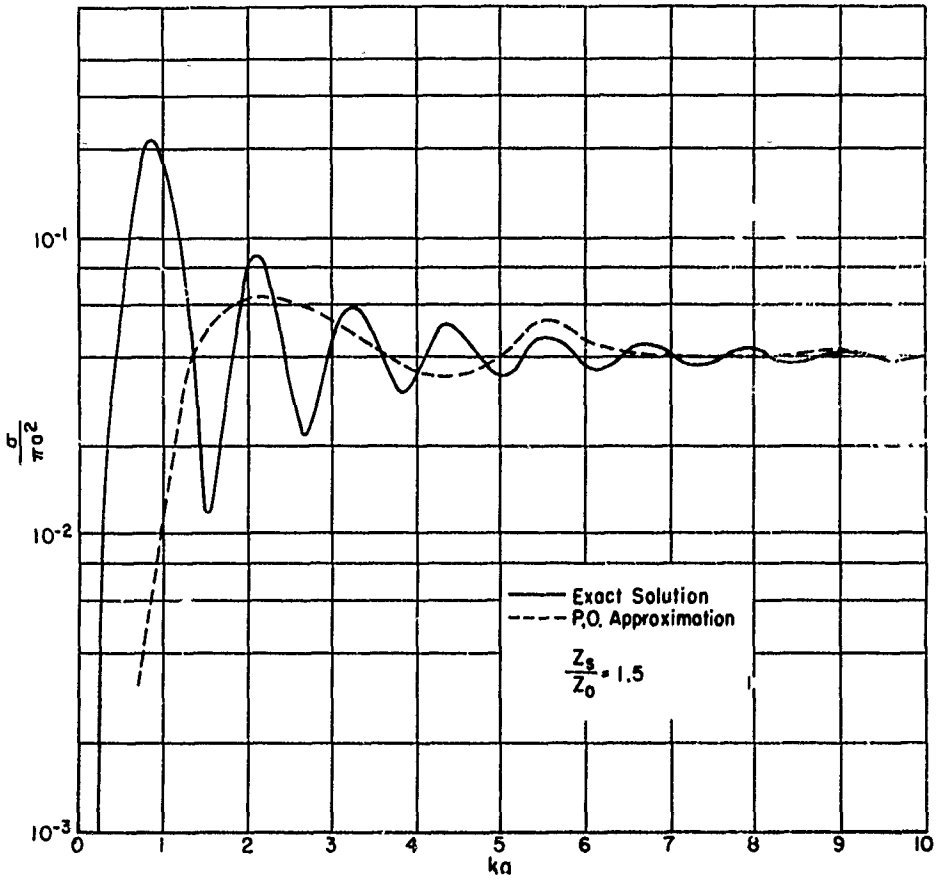

Fig. 24. Exact and approximate theoretical echo area of a sphere under impedance boundary conditions for a surface to free space impedance ratio of 1.5.

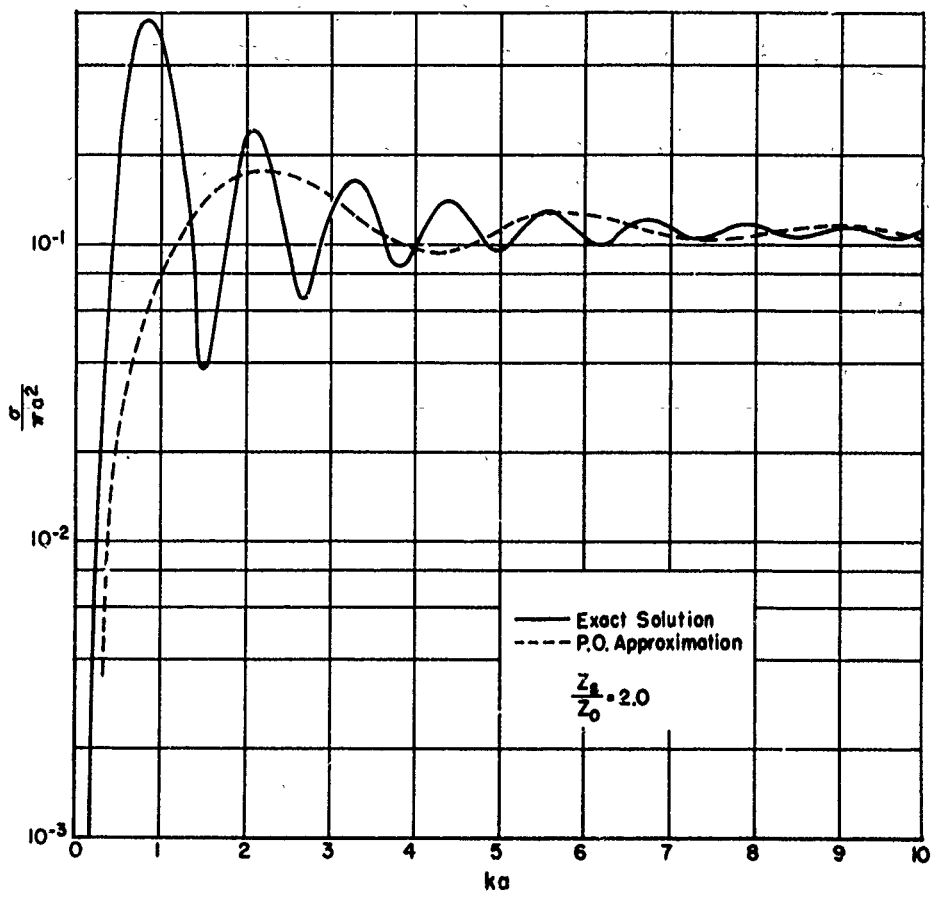

Fig. 25. Exact and approximate theoretical echo area of a sphere under impedance boundary conditions for a surface to free space impedance ratio of 2.0.

CHAPTER IV
BISTATIC CROSS-SECTIONS

A. Semi-Infinite Cones

From Eq. (52), the E-plane cross-section of the semi-infinite cone shown in Fig. 2 is given by,

$$(91)\quad \underset{\text{E-plane}}{\sigma'(\beta)} = 4\pi k^2 \tan^4\theta_o \left| \left[\frac{z_s - z_o \cos\beta \tan\theta_o}{z_s + z_o \tan\theta_o} \right] \int_o^\infty z J_1'(Bz) e^{jAz}\, dz \right.$$

$$- \left[\frac{z_o \cos\beta - z_s \tan\theta_o}{z_o + z_s \tan\theta_o} \right] \int_o^\infty \frac{J_1(Bz)}{B}\, e^{jAz}\, dz +$$

$$\left. \frac{j \sin\beta\, z_o}{z_s + z_o \tan\theta_o} \int_o^\infty z\, J_1(Bz) e^{jAz}\, dz \right|^2 ,$$

where

$$B = k \sin\beta \tan\theta_o, \qquad A = k(\cos\beta + 1).$$

Using the relations,[18]

$$\int_o^\infty e^{-at} J_\nu(bt)\, dt = \frac{\{\sqrt{a^2+b^2} - a\}^\nu}{b^\nu \sqrt{a^2+b^2}} ,$$

$$(92)\quad \int_o^\infty e^{-at} J_\nu(bt) t^\nu\, dt = \frac{(2b)^\nu \Gamma(\nu + \tfrac{1}{2})}{(a^2+b^2)^{\nu+\frac{1}{2}} \sqrt{\pi}} ,$$

$$\int_o^\infty e^{-at} J_\nu(bt) t^{\nu+1}\, dt = \frac{2a(2b)^\nu \Gamma(\nu + \tfrac{3}{2})}{(a^2+b^2)^{\nu+\frac{3}{2}} \sqrt{\pi}} ,$$

yields,

$$(93)\quad \underset{\text{E-plane}}{\sigma'(\beta)} = 4\pi k^2 \tan^4\theta_o \left| \left[\frac{1-\frac{z_o}{z_s}\cos\beta\,\tan\theta_o}{1+\frac{z_o}{z_s}\tan\theta_o}\right]\left\{\frac{-jA}{(B^2-A^2)^{\frac{3}{2}}} - \frac{(\sqrt{B^2-A^2}+jA)}{B^2\sqrt{B^2-A^2}}\right\}\right.$$

$$-\left[\frac{\cos\beta - \frac{z_s}{z_o}\tan\theta_o}{1+\frac{z_s}{z_o}\tan\theta_o}\right]\frac{(\sqrt{B^2-A^2}+jA)}{B^2\sqrt{B^2-A^2}} +$$

$$\left. j\left[\frac{\sin\beta\,\frac{z_o}{z_s}}{1+\frac{z_o}{z_s}\tan\theta_o}\right]\frac{B}{(B^2-A^2)^{\frac{3}{2}}}\right|^2 .$$

Setting $z_s = 0$,

$$(94)\quad \left.\frac{\sigma'_M(\beta)}{\lambda^2}\right|_{\text{E-plane}} = \frac{\tan^4\theta_o(\cos\beta+1)^2}{\pi\left|\sin^2\beta\tan^2\theta_o-(\cos\beta+1)^2\right|^3} .$$

From Eq. (51), the H-plane cross-section is given by,

$$(95)\quad \underset{\text{H-plane}}{\sigma'(\beta)} = 4\pi k^2 \tan^4\theta_o \left| \left[\frac{1-\frac{z_s}{z_o}\cos\beta\,\tan\theta_o}{1+\frac{z_s}{z_o}\tan\theta_o}\right]\left\{\frac{-jA}{(B^2-A^2)^{\frac{3}{2}}} - \frac{-(\sqrt{B^2-A^2}+jA)}{B^2\sqrt{B^2-A^2}}\right\}\right.$$

$$\left[\frac{\cos\beta - \frac{z_o}{z_s}\tan\theta_o}{1+\frac{z_o}{z_s}\tan\theta_o}\right]\frac{(\sqrt{B^2-A^2}+jA)}{B^2\sqrt{B^2-A^2}} +$$

$$\left. j\left[\frac{\sin\beta\,\frac{z_s}{z_o}}{1+\frac{z_s}{z_o}\tan\theta_o}\right]\frac{B}{(B^2-A^2)^{\frac{3}{2}}}\right|^2 .$$

The E- and H-plane scattering cross-sections of a 10 degree semi-infinite cone for impedance ratios, z_s/z_o, of 0, 0.5, and 1 are shown in Figs. 26 and 27, respectively.

B. Double Cones (Conducting)

If the coordinate system shown in Fig. 4 is translated, $(z \rightarrow z-b)$ then,

$$(96)\quad \alpha(z) = \begin{cases} \tan\theta_o(z+b) & -b \le z \le 0, \\ -\tan\theta_1(z-c) & 0 \le z \le c \end{cases}.$$

The results from Eqs. (52) and (54) will be identical, so from Eq. (52),

$$(97)\quad \sigma'_M(\beta) = 4\pi k^2 \left| -\int_o^{-b} \tan^2\theta_o(z+b) e^{jkz(\cos\beta+1)} J_o[k\sin\beta\tan\theta_o(z+b)]\,dz + \int_o^{c} \tan^2\theta_1(z-c) e^{jkz(\cos\beta+1)} J_o[k\sin\beta\tan\theta_o(z-c)]\,dz \right|^2,$$

a change of variable gives,

$$(98)\quad \sigma'_M(\beta) = 4\pi k^2 \left| \tan^2\theta_o \left\{ e^{-jAb} \int_o^{b} x\, e^{jAx} J_o[\Gamma x]\,dx \right\} - \tan^2\theta_1 \left\{ e^{-jAc} \int_o^{c} x\, e^{jAx} J_o[Dx]\,dx \right\}^* \right|^2,$$

where $A = k(\cos\beta+1)$, $B = -k\sin\beta\tan\theta_o$, $D = k\sin\beta\tan\theta_1$, and ν^* denotes the complex conjugate of ν. It is shown in Appendix A that

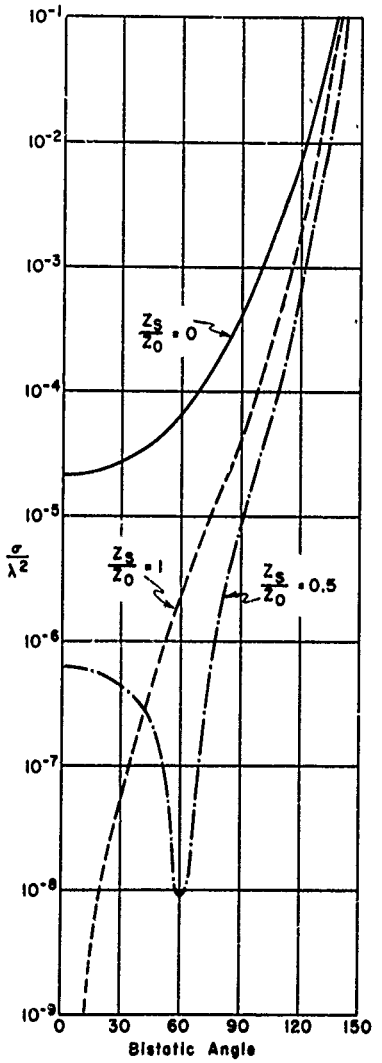

Fig. 26. Bistatic E-plane cross-section, for axial incidence, of a 10 degree semi-infinite cone for surface to free space impedance ratios of 0, 0.5, and 1.

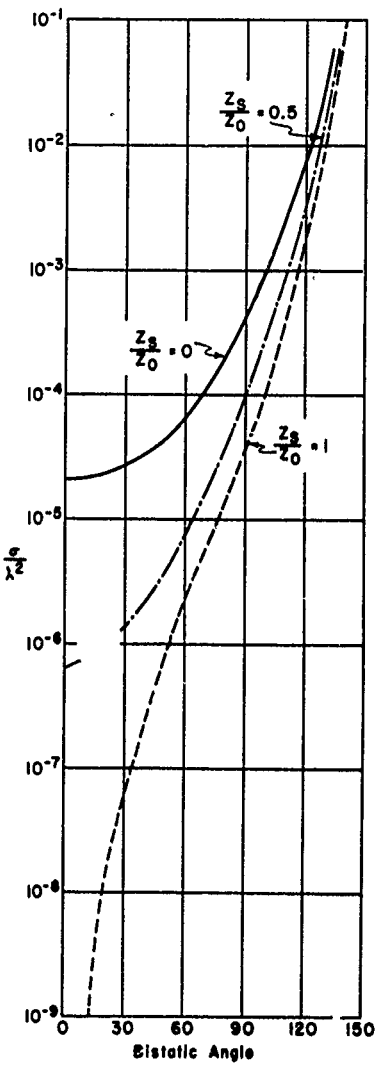

Fig. 27. Bistatic H-plane cross-section, for axial incidence, of a 10 degree semi-infinite cone for surface to free space impedance rations of 0, .5, and 1.

$$(99)\quad \int_o^a u\,J_o(u)e^{jku}\,du = \frac{1}{1-k^2}\left\{u\,J_1(u)e^{jku}\Big|_o^a + jku\,J_o(u)e^{jku}\Big|_o^a - jk\int_o^a J_o(u)e^{jku}\,du\right\},$$

hence,

$$(100)\quad \sigma'_M(\beta) = 4\pi k^2\left|\frac{\tan^2\theta_o}{(B^2-A^2)}\left\{BbJ_1(Bb)+jAbJ_o(Bb)-je^{-jAb}\int_o^{Ab}J_o\left(\frac{B}{A}x\right)e^{jx}\,dx\right\}-\frac{\tan^2\theta_1}{D^2-A^2}\left\{DcJ_1(Dc)+jAcJ_o(Dc)-je^{-jAc}\int_o^{Ac}J_o\left(\frac{D}{A}x\right)e^{jx}dx\right\}^*\right|^2 .$$

The integral

$$\int_o^a J_o(\lambda u)e^{ju}du$$

is tabulated[5] as

$$\int_o^a J_o(\lambda u)e^{ju}\,du = J_c(\lambda,a) + jJ_s(\lambda,a).$$

Curves of $J_c(\lambda,a)$ and $J_s(\lambda,a)$ as a function of a with the parameter λ are shown in Appendix C. If the double cone is symmetric, then $b = c$, $D = -B$, and $\theta_1 = \theta_o$. From Eq. (100) the bistatic cross-section of a symmetric double cone is obtained as,

$$(101)\quad \sigma_M(\beta) = \frac{4\pi k^2 \tan^4 \theta_o}{[B^2 - A^2]^2} \left| j2AbJ_o(Bb) - je^{-jAb} \left[J_c\left(\frac{B}{A}, Ab\right) + jJ_s\left(\frac{B}{A}, Ab\right) \right] - \right.$$

$$\left. je^{jAb} \left[J_c\left(\frac{B}{A}, Ab\right) - jJ_s\left(\frac{B}{A}, Ab\right) \right] \right|^2 .$$

In the limit as $kb \to 0$,

$$(102)\quad \sigma_M(\beta)_{kb \to 0} \frac{4\pi k^4 \tan^4 \theta_o}{[\sin^2 \beta \tan^2 \theta_o - (\cos\beta + 1)^2]^2} \frac{(\cos\beta + 1)^3 b^3}{3} \cdot$$

$$\cdot \left[1 - \frac{\sin^2 \beta \tan^2 \theta_o}{(\cos\beta + 1)^2} \right]^2 ,$$

for large kb,

$$(103)\quad \frac{\sigma_M(\beta)}{\pi a^2} \simeq \frac{4\tan^2 \theta_o}{[\sin^2 \beta \tan^2 \theta_o - (\cos\beta + 1)^2]} \{2(\cos\beta + 1) J_o(kb \sin\beta \tan\theta_o)\}$$

The bistatic cross-section of a 20 degree half angle symmetric double cone ($b = 1.83\lambda$, $c = .665\lambda$) as calculated from Eq. (101) is shown in Fig. 28. Figure 28 also gives the experimentally measured E- and H-plane cross-sections of this cone. Reasonable, good agreement is obtained between the measured E-plane cross-section and the theoretical cross-section.

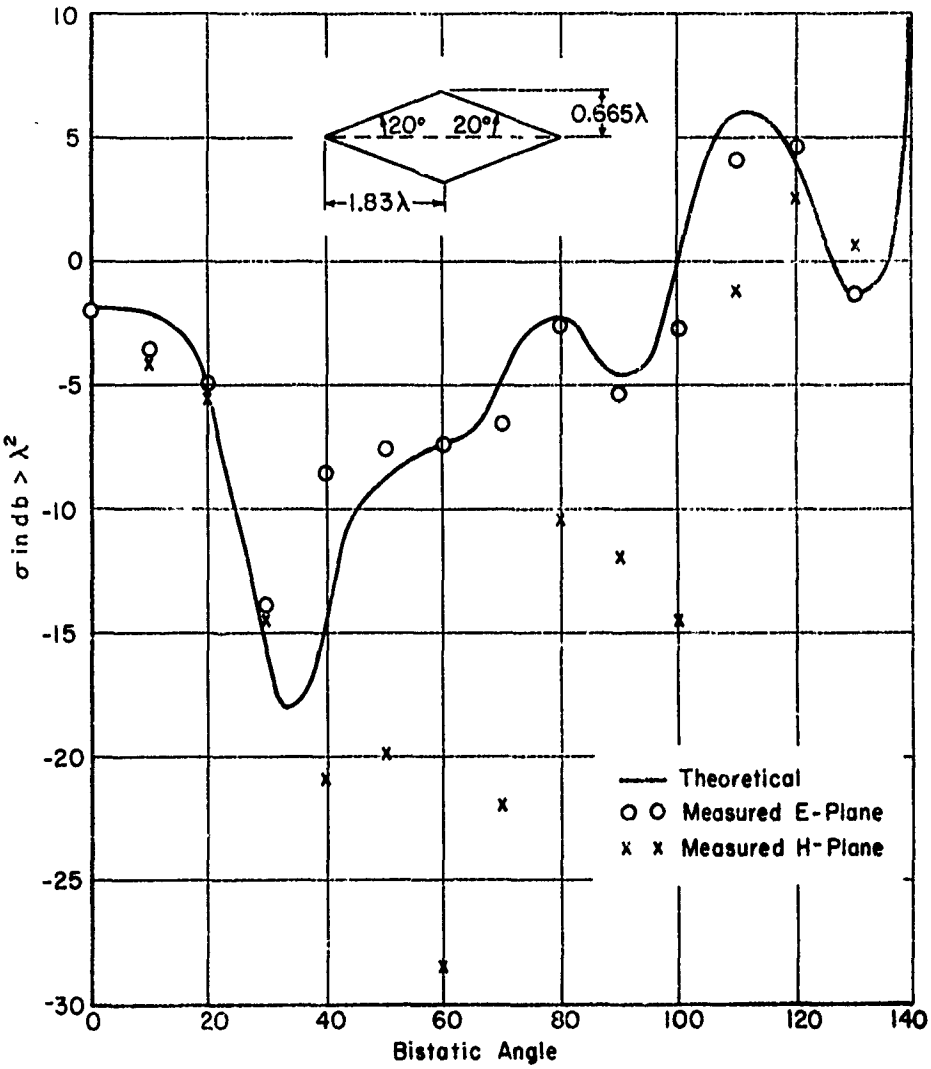

Fig. 28. Theoretical E-plane and measured E- and H-plane bistatic cross-sections of a 20 degree half angle symmetric double cone for axial incidence.

C. Semi-Infinite Cylinder with a Cone Cap

If θ_1 is set equal to zero in Eq. (100), the bistatic H-plane cross-section of the semi-infinite cylinder capped with a cone shown in Fig. 15 is obtained as,

$$(104)\quad \underset{\text{H-plane}}{\sigma'_M(\beta)} = \frac{4\pi k^2 \tan^4\theta_o}{[B^2 - A^2]^2} \Big| BbJ_1(Bb)+jAbJ_o(Bb)-je^{-jAb}\cdot \left\{J_c[B/A, Ab] + jJ_s[B/A, Ab]\right\}\Big|^2 .$$

In the limit as $kb \to 0$,

$$(105)\quad \underset{\text{H-plane}}{\sigma'_M(\beta)} \xrightarrow[kb \to 0]{} \pi a^2 (kb)^2 \tan^2\theta_o .$$

For large kb,

$$(106)\quad \underset{\text{H-plane}}{\sigma'_M(\beta)} \xrightarrow[kb \to \infty]{} \frac{4\pi a^2 \tan^2\theta_o}{[\sin^2\beta \tan\theta_o - (\cos\beta + 1)^2]^2} \left\{[\sin\beta \tan\theta_o J_1(kb \sin\beta \tan\theta_o)]^2 + [(\cos\beta+1)J_o(kb \sin\beta \tan\theta_o)]^2\right\}.$$

From Eq. (54), the bistatic E-plane cross-section is,

$$(107)\quad \underset{\text{E-plane}}{\sigma'_M(\beta)} = 4\pi k^2 \tan^2\theta_o \left| \left\{\frac{\cos\beta \tan\theta_o}{B^2 - A^2} + \frac{\sin\beta\, B}{A(B^2 - A^2)}\right\} \left[jJ_c[B/A, Ab] - J_s[B/A, Ab] - jAbJ_o(Bb)e^{jAb} - BbJ_1(Bb)e^{jAb}\right] + \frac{\sin\beta b}{A} J_1(Bb)e^{jAb}\right|^2 .$$

In the limit as $kb \to 0$,

$$(108)\quad \sigma'_M(\beta) \xrightarrow[kb \to 0]{} \frac{4\pi k^2 \tan^4\theta_o (1+\cos\beta)^2}{[\sin\beta(\tan^2\theta_o - 1) - 2\cos\beta]^2}$$

For large kb,

$$(109)\quad \frac{\sigma'_M(\beta)}{\pi a^2}\ \underset{kb \to \infty}{\longrightarrow}\ 4\left|\cos Ab\left\{\frac{\sin\beta\, J_1(Bb)}{\cos\beta + 1} - \frac{\sin\beta\tan^2\theta_o J_1(Bb) + j(\cos\beta+1)\tan\theta_o J_o(Bb)}{\sin^2\beta\tan^2\theta_o - (\cos\beta+1)^2}\right\}\right.$$
$$\left. + \sin Ab\left\{\frac{j\sin\beta\, J_1(Bb)}{\cos\beta+1} + \frac{\tan\theta_o(\cos\beta+1)J_o(Bb) - j\sin\beta\tan^2\theta_o J_1(Bb)}{\sin^2\beta\tan^2\theta_o - (\cos\beta+1)^2}\right\}\right|^2 .$$

The E- and H-plane scattering cross-sections of a semi-infinite cylinder capped with a 20 degree half angle cone (kb = 11.5) are shown in Fig. 29.

D. Finite Cylinder with Cone Caps

A finite cylinder with cone caps is shown in Fig. 30. As was the case with the double cones, only one bistatic cross-section is predicted for this target by the long, thin body approximation.

From Fig. 30,

$$(110)\quad \alpha(z) = \begin{cases} \tan\theta_o(b+z) & -b \le z \le 0 \\ a & 0 \le z \le N \\ \tan\theta_1(c-z) & N \le z \le c \end{cases} .$$

Using Eq. (52),

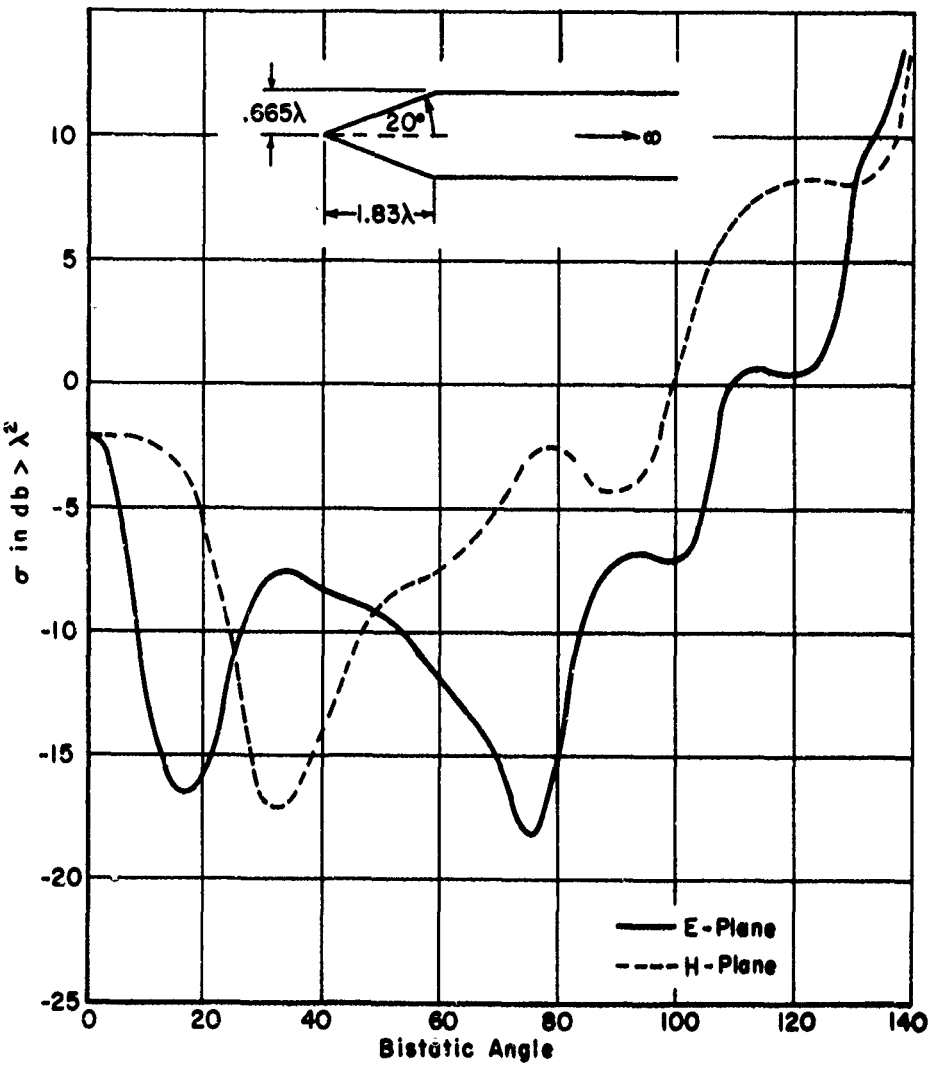

Fig. 29. Theoretical E- and H-plane bistatic cross-sections of a semi-infinite cylinder capped with a 20 degree half angle cone for axial incidence.

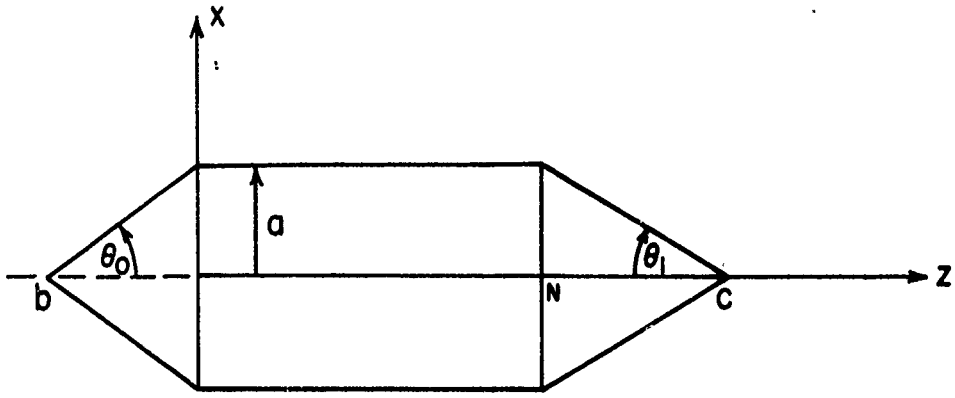

Fig. 30. Finite cylinder with cone caps.

$$(111)\quad \sigma'_M(\beta) = 4\pi k^2 \left| \tan^2\theta_o \int_{-b}^{o} (b+z) J_o[k\tan\theta_o \sin\beta(b+z)] e^{jkz(\cos\beta+1)} dz \right.$$

$$\left. -\tan^2\theta_1 \int_N^c (c-z) J_o[k\tan\theta_1 \sin\beta(c-z)] e^{jkz(\cos\beta+1)} dz \right|^2 .$$

A change of variable gives,

$$(112)\quad \sigma'_M(\beta) = 4\pi k^2 \left| \tan^2\theta_o e^{-jAb} \int_o^b x\, J_o(Bx)\, e^{jAx} dx \right.$$

$$\left. -\tan^2\theta_1 \left\{ e^{-jAc} \int_o^{c-N} x\, J_o(Dx) e^{jAx} dx \right\}^* \right|^2 ,$$

where

$$A = k(\cos\beta + 1)$$

$$B = k \sin\beta \tan\theta_o$$

$$D = k \sin\beta \tan\theta_1 ,$$

and the integrals were evaluated for double cones. If the cone caps are identical, ($\theta_o = \theta_1$) there is obtained,

$$(113)\quad \sigma'_M(\beta) = \frac{4\pi k^2 \tan^4\theta_o}{[B^2 - A^2]^2}\left| Bb\,J_1(Bb)+jAb\,J_o(Bb)-je^{-jAb}\right.$$

$$\left.+e^{jAN}\left[-BbJ_1(Bb)+jAbJ_o(Bb)-je^{jAb}\left\{J_c[B/A, Ab]-jJ_s[B/A, Ab]\right\}\right]\right|^2 .$$

It can be seen from Eq. (113) that for particular lengths, N, the bistatic cross-section of a finite cylinder with cone caps reduces to that for the double cone. Setting the bistatic angle to zero in Eq. (112), the axial backscatter from a finite cylinder with cone caps is obtained.

$$(114)\quad \sigma'_M(0) = \frac{\tan^2\theta_o}{4(kb)^2}\left| -e^{j2kb}(j2kb-1)-1\right.$$

$$\left.+\frac{\tan^2\theta_1}{\tan^2\theta_o}\left\{-e^{j2kN}\left[j2k(c-N)+1\right]+e^{j2kc}\right\}\right|^2 .$$

The bistatic cross-section of a finite cylinder with 20^o cone caps is shown in Fig. 31. In Appendix B, the axial echo areas of a double cone, semi-infinite cylinder with cone cap, and finite cylinder with cone caps are compared.

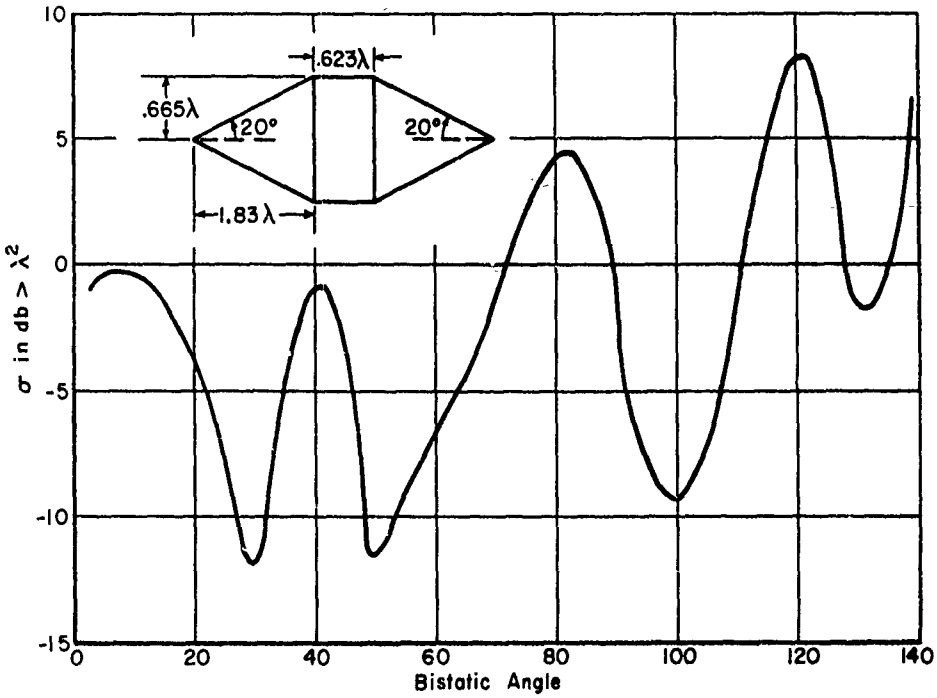

Fig. 31. Theoretical bistatic cross-section of a finite cylinder capped by 20° half angle cones for axial incidence.

CHAPTER V
DISCUSSION AND CONCLUSIONS

Four limitations or failings are generally attributed to the physical optics method; they are: (1) Incorrect results in the Rayleigh and low resonance regions and hence a limitation on target size, (2) Reciprocity is not satisfied, (3) The polarization dependence for backscatter is not dependent on scatter shape and incorrect in many cases, and (4) The target shape in the shadow region is not taken into account. Obviously, the limitation of incorrect polarization dependence for backscatter does not apply here since axial incidence and rotationally symmetric targets are specified. However, the other restrictions given above do apply to Eqs. (43), (44), and (46), the standard physical optics results. The inclusion of a class of imperfectly conducting targets with an arbitrary surface impedance does not alter these restrictions. In any case, a target which satisfies the conditions for application of the impedance boundary condition can never become a Rayleigh scatterer. It has been shown,[2] that the physical optics method does not, in general, satisfy reciprocity, and this restriction clearly applies to the modification developed here. The restriction on target size, and the failure to consider the target shape in the shadow region are directly related. The low frequency response predicted by physical optics is

incorrect because the currents induced on the shadow portion of the scatterer are not considered. When the target size in wavelengths becomes sufficiently large, these shadow currents are essentially zero and the physical optics result is correct. The works of Foch,[8] Keller,[25] and Kennaugh,[23,24] have been concerned, directly or indirectly, with the problem of correctly predicting the low frequency response. Clearly, the method of accounting for the shadow currents used here lacks the sophistication and generality of the above techniques, but for a restricted class of targets and a particular choice of the source location, the simple expedient of extending the physical optics currents over the entire scatterer has been shown to yield surprisingly good results.

Two sets of equations predicting the scattering for axial incidence from rotationally symmetric targets have been developed. The standard (or rate of change of area in the receiver direction over the illuminated target area) physical optics approximation has been extended to include a class of imperfectly conducting targets. It is important to note that it is not necessary that the imperfectly conducting target be homogeneous; the equations are applicable to layered targets (e.g., absorber coated) as long as the exterior surface satisfies the Leontovich[6] conditions. Figures 26 and 27 which compare the exact and approximation solutions for back-scatter from spheres

indicates the validity of the approximation. Emphasis in this report, however, has been on the second set of derived equations which are applicable to long, thin, Adachi[3] type targets. In this case, Adachi's solution, or rather the first order approximation to it, has been extended to imperfectly conducting targets and to the bistatic configuration. Unfortunately, the long, thin target modification of the physical optics approximation removes the polarization dependence of the solution for finite scatterers and only one cross section is predicted. Experimental evidence has thus far supported the postulate that the predicted cross-section is valid for the E-plane, but additional verification is necessary before this conclusion may be stated in general. In Fig. 12, excellent agreement between the theoretical and measured axial backscatter from symmetric and non-symmetric conducting double cones is obtained. The validity of the bistatic solution is demonstrated in Fig. 30, where the measured and theoretical E-plane cross-sections of a symmetric double cone are compared. Thus, an exceedingly simple expression has been derived which is not subject, at least as stringently, to two of the most serious limitations of physical optics. The bistatic solution, however, does not have a polarization dependence for finite targets, and the results are incorrect, in general, for bistatic angles greater than the specular reflection angle.

The approximate Fresnel reflection coefficients derived in Chapter II, and applied to the physical optics scattering approximation, when compared to the accurate Fresnel expressions[8] exhibit an error of the order of $(\cos^2\theta)/(\mu_r\epsilon_r)$. ($\theta$ is defined in Fig. 1, μ_r, ϵ_r are, respectively, the relative permeability and permittivity of the target medium). Obviously, the approximate reflection coefficients are least valid for long, thin targets with apices, but since a large $\mu\epsilon$ product was assumed, the condition, $(\cos^2\theta)/(\mu_r\epsilon_r) \ll 1$, should hold even for these targets.

The general expressions for axial backscatter in Eqs. (55) and (56) offer a means for determining the terminating shape necessary to minimize the axial return. That is, given a fixed target shape in the illuminated region, the terminating shape in the shadow region which will minimize the axial return can be determined. This work is beyond the scope of this report, but both a rigorous analysis by the calculus of variations, and a simple assumed polynomial solution appear to be feasible. Keller[19] has made some recommendations concerning this problem which the results in Eq. (56) appear to support.

In summary, the following conclusions may be stated. A physical optics approximation to the scattering, for axial incidence, from rotationally symmetric targets with an arbitrary surface

impedance has been derived. These expressions are subject to the usual physical optics limitations.

A modified physical cptics approximation to the scattering, for axial incidence, from rotationally symmetric targets with an arbitrary surface impedance applicable to long, thin targets with apices has been derived. These results give only the monostatic and E-plane bistatic cross-sections, and are of limited usefulness since axial incidence is assumed, but the predicted scattering for conducting targets agrees remarkably well with measured data. In the case of imperfectly conducting long, thin targets, no experimental verification of the derived equations has been obtained and the results are still in question. The modified physical optics approximation assumes that the diffracted field in the shadow region has a wave-number very near that of the incident field, and for lossy targets this may not be true even for very thin scatterers.

For targets of the long, thin class with apices, the axial back-scatter is single-valued, that is, the axial backscatter from either end of a non-symmetric double cone, for example, is the same.

For targets of the long, thin class with apices, the periodicity of the frequency response is dictated by the electrical length from the nose to any discontinuities in the slope of the target, the overall electrical length, and if the slope of the target is not constant, by the

surface impedance of the scatterer. Thus, for example, the period of a conducting double cone will be approximately twice that of a conducting double cone of the same dimensions for which the wedge where the cone bases join has been smoothed.

For bistatic angles greater than the specular reflection angle, the long, thin target equations led to questionable cross-sections, and the standard physical optics results should be used. A more reasonable expression for the forward scatter cross-section is available from the variational result in Eq. (70).

The surprising success, for a particular class of conducting targets, of an exceedingly simple modification of physical optics in accounting for the shape of the target in the shadow region indicates that perhaps the physical optics method has not yet been fully utilized in the approximate solution of scattering problems. It may be merely fortuitous that this modification works so well, but some effort should be expended in an attempt to extend the results to a more general class of targets, and ultimately to removing the source from the symmetry axis.

BIBLIOGRAPHY

1. Eberle, Jon, "Extension of the Physical Optics Approximation to Small Bodies," Report 827-6, 1 November 1959, Antenna Laboratory, The Ohio State University Research Foundation; prepared under Contract AF 19(604)-3501, Air Force Cambridge Research Center, Air Research and Development Command, Laurence G. Hanscom Field, Bedford, Massachusetts.

2. Siegel, K. M., et al., "Theoretical Cross-Sections as a Function of Separation Angle Between Transmitter and Receiver at Small Wavelengths," Studies in Radar Cross-Sections VIII, October 1953, Willow Run Research Center, Engineering Research Institute, University of Michigan.

3. Adachi, Saburo, "The Nose-On Echo Area of Axially Symmetric Thin Bodies Having Sharp Apices," Report 925-1, 31 March 1960, Antenna Laboratory, The Ohio State University Research Foundation; prepared under Contract AF 30(602)-2042, Rome Air Development Center, Air Research and Development Command, Griffiss Air Force Base, New York.

4. Peters, L., Jr., "End-Fire Echo Area of Long, Thin Bodies," IRE Trans. AP-6, No. 1, pp. 133-139 (1958).

5. "Tables of $\int_0^u J_0(\lambda x)e^{jx}dx$," Report 510-10, 15 June 1954, Antenna Laboratory, The Ohio State University Research Foundation; prepared under Contract DA 36-039 sc15554, Signal Corps Supply Agency, Laboratory Procurement Office, Fort Monmouth, New Jersey.

6. Stratton, J. A., Electromagnetic Theory, McGraw-Hill Book Co., Inc., p. 466, 1941.

7. Stratton, op. cit., p. 604.

8. Leontovich, M. A., Appendix to "Diffraction, Refraction, and Reflection of Radio Waves," thirteen papers by V. A. Fock, June 1957, Antenna Laboratory, Electronics Research Directorate, Air Force Cambridge Research Center, Air Research and Development Command, Bedford, Massachusetts.

9. Stratton, op. cit., p. 419.

10. Stratton, op. cit., p. 372.

11. Mentzner, J. R., Scattering and Diffraction of Radio Waves, Pergamon Press Ltd., London, 1955.

12. Stratton, op. cit., p. 360.

13. Storer, J. E. and Sevick, J., "A General Theory of Plane-Wave Scattering from Finite Conducting Obstacles with Application to the Two Antenna Problems," Journal of Applied Physics, Vol. 25, pp. 369-376, 1954.

14. Morse and Feshbach, Methods of Theoretical Physics, McGraw-Hill Book Co., Inc., p. 1069, 1953.

15. Garbacz, R., "The Bistatic Scattering from a Class of Lossy Dielectric Spheres with Surface Impedance Boundary Conditions," Report 925-5, 15 January 1961, Antenna Laboratory, The Ohio State University Research Foundation; prepared under Contract AF 30(602)-2042, Rome Air Development Center, Air Research and Development Command, Griffiss Air Force Base, New York.

16. Marcinkowski, C. J., "Diffraction by an Absorbing Half-Plane," Research Report R-750-59, PIB-678, Air Force Cambridge Research Center, Air Research and Development Command, Laurence G. Hanscom Field, Bedford, Massachusetts, 29 September 1959.

17. Jahnke, E. and Emde, F., "Tables of Functions," Dover Publications, p. 3, 1945.

18. Watson, G. N., A Treatise on the Theory of Bessel Functions, The MacMillan Company, p. 386, 1945.

19. Keller, J. B., "Backscattering from a Finite Cone," IRE Transactions on Antennas and Propagation, Vol. AP-8, No. 2, March 1960.

20. Stratton, op. cit., p. 359.

21. Jahnke, op. cit., p. 36.

22. Eberle, J. and St. Clair, R., "Echo Area of Combinations of Cones, Spheroids and Hemispheres as a Function of Bistatic Angle and Target Aspect," Report 1073-1, 30 June 1960, Antenna Laboratory, The Ohio State University Research Foundation; prepared under Contract AF 19(604)-6157, Air Force Cambridge Research Center, Air Research and Development Command, Laurence G. Hanscom Field, Bedford, Massachusetts.

23. Kennaugh, E. M. and Cosgriff, R. L., "The Use of Impulse Response in Electromagnetic Scattering Problems," IRE National Convention Record, Part I, March 1958.

24. Kennaugh, E. M., "The Scattering of Transient Electromagnetic Waves by Finite Bodies," presented at URSI-IRE Fall Meeting, National Bureau of Standards, Boulder, Colorado.

25. Keller, J. B., "A Geometric Theory of Diffraction," Research Report No. EM-115, New York University, July 1958.

26. Hiatt, R. E., Siegel, K. M., and Weil, H., "Forward Scattering by Coated Objects Illuminated by Short Wavelength Radar," Proceedings of IRE, Vol. 48, No. 9, 1960.

ACKNOWLEDGMENT

It is a pleasure to acknowledge the suggestions and criticisms of Dr. E. M. Kennaugh, Dr. C. A. Levis, and Mr. R. J. Garbacz. The detailed checking by Mr. Garbacz of a major portion of this report is particularly appreciated. The numerical computations were done by Mrs. Frances Phillips, and the experimental measurements were performed by Mr. J. Gillard.

APPENDIX A.* EVALUATION OF $I = \int_{\alpha_1}^{\alpha_2} u J_o(u) e^{jku}\, du$

From Eq. (57), the integral may be written as

$$I = \int_{\alpha_1}^{\alpha_2} \frac{d}{du} [u J_1(u)] e^{jku}\, du. \tag{A-1}$$

An integration by parts gives,

$$I = u J_1(u) e^{jku} \Big|_{\alpha_1}^{\alpha_2} - jk \int_{\alpha_1}^{\alpha_2} u J_1(u) e^{jku}\, du. \tag{A-2}$$

The integral may also be written as,

$$I = \int_{\alpha_1}^{\alpha_2} J_o(u) \left\{ \frac{d}{du} \left[\frac{u}{jk} e^{jku} \right] - \frac{1}{jk} e^{jku} \right\} du, \tag{A-3}$$

and an integration by parts gives

$$I = -\frac{1}{jk} \int_{\alpha_1}^{\alpha_2} J_o(u) e^{jku}\, du + \frac{u}{jk} e^{jku} J_o(u) \Big|_{\alpha_1}^{\alpha_2} + \frac{1}{jk} \int_{\alpha_1}^{\alpha_2} u J_1(u) e^{jku}\, du . \tag{A-4}$$

Multiplying Eq. (A-4) by $(jk)^2$ and adding to Eq. (A-2),

---

*The author is indebted to Dr. E. M. Kennaugh for this derivation.

(A-5) $$I = \frac{I}{1 + (jk)^2} \left\{ u J_1(u) e^{jku} \Big|_{\alpha_1}^{\alpha_2} + jku\, J_0(u) e^{jku} \Big|_{\alpha_1}^{\alpha_2} - \right.$$

$$\left. -jk \int_{\alpha_1}^{\alpha_2} J_0(u) e^{jku}\, du \right\}$$

APPENDIX B - AXIAL BACKSCATTER OF CONE COMBINATIONS

The axial backscatter from a symmetric double cone, semi-infinite cylinder with a cone cap, and a finite cylinder with symmetric cone caps as predicted by the modified physical optics approximation is shown in Fig. A. The targets are assumed to be perfectly conducting.

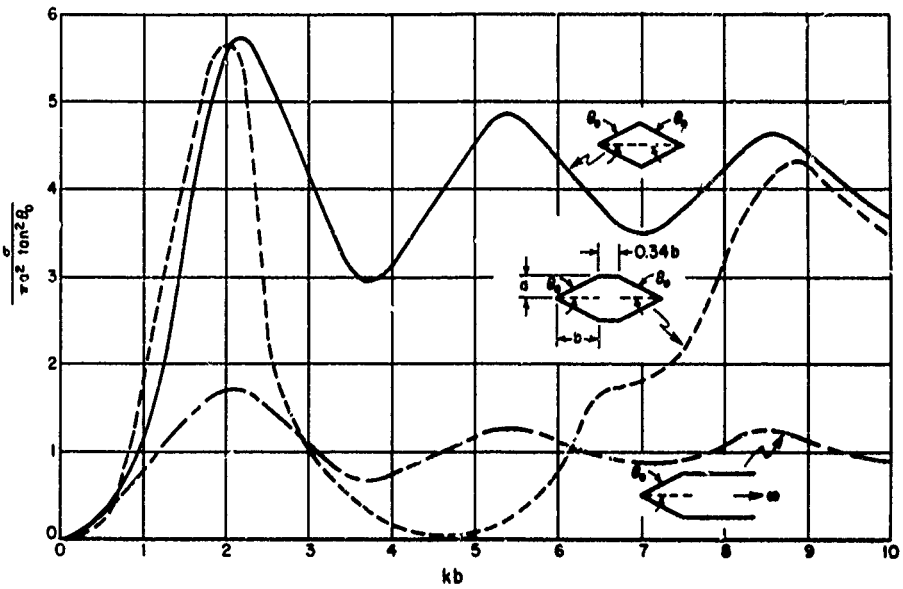

Fig. A. Normalized axial backscatter from a conducting symmetric double cone, semi-infinite cylinder with cone cap, and finite cylinder with symmetric cone caps.

APPENDIX C. CONCERNING $\int_o^u J_o(\lambda x)e^{jx}dx = J_c(\lambda, u)+j\,J_s(\lambda, u)$

As previously mentioned, tabulated values of $J_c(\lambda, u)$ and $J_s(\lambda, u)$ are available,[5] for

$$0 \leq \lambda u \leq 1.5$$

$$0 \leq \lambda \leq 10$$

$$0 \leq u \leq 1.5/\lambda.$$

The increments in λ and u in the tables make interpolation necessary, and for that purpose, the curves of $J_c(\lambda, u)$ and $J_s(\lambda, u)$ shown respectively in Figs. A-I and A-II were prepared.

When $\lambda u \geq 1.5$, the integral may be written as,

$$\text{(C-1)} \qquad \int_o^u J_o(\lambda u)e^{jx}\,dx = \int_o^{u'} J_o(\lambda x)e^{jx}\,dx + \int_{u'}^{u} \sqrt{\frac{2}{\pi\lambda x}}\cos\left[\lambda x - \frac{\pi}{4}\right] e^{jx}\,dx,$$

where $\lambda u' = 1.5$, and the asymptotic form[20] $J_o(\lambda x) = \sqrt{\frac{2}{\pi\lambda x}}\cos[\lambda x - \pi/4]$ has been used for $\lambda x > 1.5$. Since,

$$\text{(C-2)} \qquad \int_o^z \frac{e^{-it}}{\sqrt{2\pi t}}\,dt = C(z) - jS(x),$$

where C(z) and S(z) are Fresnel's integrals,

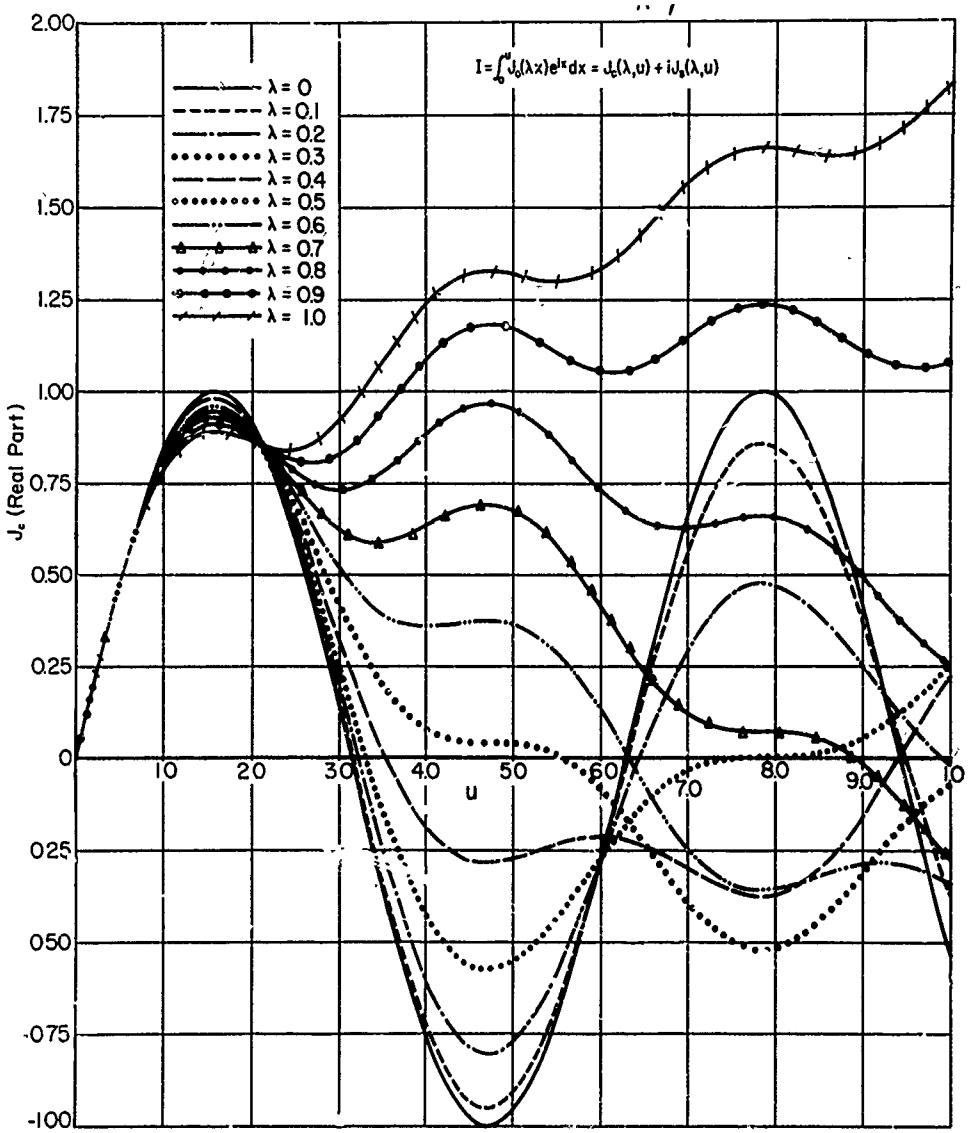

Fig. A-1. $J_c(\lambda, u)$, real part $\int_0^u J_0(\lambda x) e^{jx}\, dx$,
as a function of u with the parameter λ.

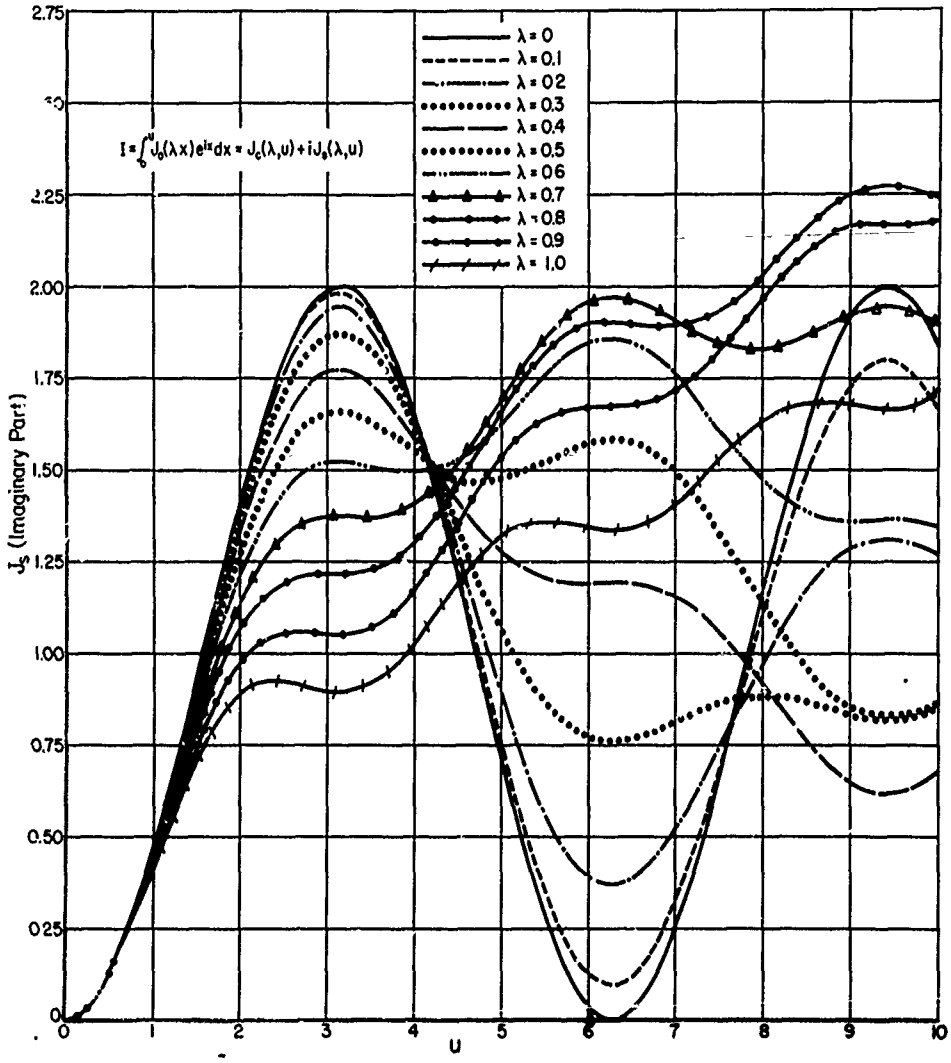

Fig. A-2. $J_s(\lambda, u)$, imaginary part of $\int_0^u J_0(\lambda x) e^{jx}\, dx$, as a function of u with the parameter λ.

$$(C\text{-}3)\quad \int_0^u J_o(\lambda x)e^{jx}\,dx = J_c(\lambda, u') + j\,J_s(\lambda, u') +$$

$$\frac{(1-j)}{\sqrt{2\lambda(\lambda+1)}}\left[C[(\lambda+1)u]-C[(\lambda+1)u']+jS[(\lambda+1)u]-jS[(\lambda+1)u']\right]+$$

$$\frac{(1+j)}{\sqrt{2\lambda(\lambda-1)}}\left[C[(\lambda-1)u]-C[(\lambda-1)u']-jS[(\lambda-1)u]+jS[(\lambda-1)u']\right] .$$

C(z) and S(z) are tabulated in Reference 17.